DESIGN CONCEPTS FOR BOREX

(Boron Solar Neutrino Experiment)

R. S. Raghavan, J. W. Mitchell, E. A. Chandross and B. G. Cortez
AT&T Bell Laboratories, Murray Hill, New Jersey 07974
and
R. Steinberg and C. E. Lane
Department of Physics, Drexel University, Philadelphia Pa. 19104

ABSTRACT

The Boron solar neutrino experiment (Borex) aims at spectroscopic observation of neutrinos from the decay of ^{8}B in the sun using direct-counting modes based on neutral and charged weak currents. This report is a study of how its goals can be realized in practice. A conceptual design for Borex based on a large tank of boron loaded liquid scintillator viewed by a number of phototubes, is outlined. The scintillator liquids are commercially available in the required quantity and quality. Recent tests indicate that these liquids can also be made with the high radio-purity required for the operation of Borex. Assuming that test purities can be realized in the full-scale detector, the external background can be controlled sufficiently to enable observation of good quality signals of solar neutrinos. The design incorporates signatures for demonstrating neutrino origin of the signals (besides specifying flavor, neutrino/antineutrino type and nearly complete spectral profiles) as well as vetoes demonstrating non-neutrino origin of events. The experiment can be carried out in an underground facility at a depth similar to that at Gran Sasso.

AT&T BELL LABORATORIES (ATT-BX-88-01)

March 31, 1988

Table of Contents

List of Tables

List of Figures

1. Borex: Overview and Summary

The ^{11}B solar neutrino experiment (Borex)[1] [2] aims at observing neutrinos (ν) from the decay of ^{8}B in the sun using several direct-counting modes with different flavor sensitivities. First, electron neutrinos (ν_e) can be detected by inverse β-decay of ^{11}B and the spectrum of solar ν_e's arriving on earth can be recorded. Secondly, the total flux of ν's of *all* flavors can be measured by neutral current-based reactions exciting the nuclear levels of ^{11}B. Thirdly, antineutrinos ($\overline{\nu}_e$) can also be specifically and spectroscopically observed.

^{8}B neutrinos are created in the sun as electron neutrinos. By measuring the total "all-flavor" ν flux on earth, the magnitude of the original ν_e flux can be obtained irrespective of ν flavor transformations en route. The ^{8}B solar ν output is a direct and sensitive index of the central temperature of the sun. By determining the flux of only electron neutrinos at the earth and comparing it to the measured "all-flavor" flux of ν's, we can unequivocally demonstrate a depletion of the ν_e flavor due to ν oscillations during ν transport through the sun, the earth and the intervening space. Such effects of non-conservation of ν flavor directly explore new properties of the neutrino. Borex is thus equipped to probe the astrophysics and the particle physics of solar ν's independently and in a complete manner.

^{8}B solar neutrinos are of MeV energies and their flux is small. Thus, extremely low backgrounds and sensitivities typical of table-top low energy nuclear physics must be achieved in a massive detector typical of high energy particle physics. This report is a study of how this goal may be reached in the case of Borex. We develop ideas for identifying solar neutrino signals from the different detection modes as well as rejecting non-neutrino events and adopt a specific experimental approach in which these ideas can be applied effectively. The practicality of this approach and the extent to which it can attain the aims of Borex are explored by constructing and analyzing a conceptual design (CD) for this detector. A detailed examination of the problem of background in this design is made and the needs for technical sensitivities and material qualities are assessed, identifying those that are on hand and those requiring further optimization.

The central points of this report can be summarized as follows:

- Liquid scintillation spectroscopy, a robust low energy method, offers an experimental approach tailored to Borex. It can be applied to certain borated liquids which are highly transparent to scintillation light and industrially available in the large amounts required for Borex.

- Borex can be based on a conceptual design (CD) consisting of a large steel tank containing some 2 kTons of borated liquid scintillator viewed by $\sim$1450 50 cm dia. phototubes, the tank being immersed in a pool of pure water in an underground cavity.

• The design builds upon the experience of recent, large water Cerenkov detectors built to study nucleon decay. The basic difference in Borex is that, with ~ 40 times more light available in scintillation than Cerenkov emission, sensitivity can be extended to events of much lower energies and the *energy* and *spatial* resolution in general, enhanced considerably.

• The external background due to radioactivity from the steel tank, phototubes and the rock ambience can be adequately shielded. Cosmic ray muon-induced background can be suppressed provided, overburden thicknesses of the order of the Gran Sasso Laboratory are available.

• The *charged-current* signal, affected mainly by the external background, can be safely measured with high signal/noise ratio.

• The main source of background at low energies, for the *neutral current* signal, will be the trace radioactivity in the fiducial volume of the detector. Preliminary Bell Labs data[3] indicate that trace purities of the order of 10^{-15} to 10^{-16}g/g, in the range relevant to Borex, may be attainable in the boron liquids.

• At the levels of local background and spatial resolution foreseen for this conceptual design, correlations of events in time and space can be identified, facilitating signatures for specifying and sorting the different ν reactions and tags for identifying and vetoing background in Borex.

The single most important component in this design is the Boron scintillator. Its radiopurity, in particular, will determine the extent to which the physics potential of Borex can be realized in practice. Thus a main part of the development work will focus on this aspect. If the present results from laboratory tests of the radiopurity can be realized under actual field conditions, the objectives of Borex viz., observation of a nearly complete, high quality inverse β^- spectrum and the clear identification of the line features of the neutral current signals, can be fully achieved.

This report is organized as follows. The nuclear physics and the observable event rates for the various detection modes in Borex are summarized in §2 (and supplemented by App. I). The Borex CD is presented in §3, followed by §4,5 describing the scintillator characteristics and the operational detection sensitivities foreseen in Borex. Control of the external γ-ray background by the shielding architecture of the CD and by vetos of events from trace radioactivity in the fiducial volume are discussed next. Other aspects of the background problem are discussed in App. II to IV. In §7, signatures for tagging and sorting the various ν reactions are discussed. Finally, in §8, an quantitative spectral profile of the overall background is constructed and confronted with with the solar ν signal profile.

2. Solar Neutrino Detection Modes and Event Rates

2.1 Detection of ν_e by Inverse β^- Decay: This reaction, based on the weak *charged* current (CC), induces CC transitions from the ground state of the target ^{11}B to that of ^{11}C (CC(III)) as well as its excited levels at energies E'_i (CC(II) and CC(I)). (see Fig. 1 for the level scheme of the $^{11}B - {}^{11}C$ system):

$$\nu_e + {}^{11}B \rightarrow \beta^- + [\,{}^{11}C^*(E'_i) \rightarrow \gamma(E'_i) + {}^{11}C\,] \qquad (1)$$

The CC nature of these transitions dictates that they detect only *electron neutrinos* ν_e. The thresholds for the CC-transitions are given by $E_{th}=E'_i+\Delta$ where $\Delta = 1.982$ MeV, the $^{11}B-{}^{11}C$ mass-difference. In a ground-state transition CC(III), an electron of energy $E_{\beta^-} = E_\nu - E_{th}$ is emitted; in the excited state transitions CC(II) and CC(I), the β^- is accompanied by a de-excitation γ-ray of energy E'_i. The event-energy is $E = E'_i + E_{\beta^-} = E_\nu - \Delta$. The inverse β^- energy spectrum ($E_{\beta^-}=0$ to ~ 12 MeV) faithfully reflects the *solar ν_e-spectrum arriving at the detector.*

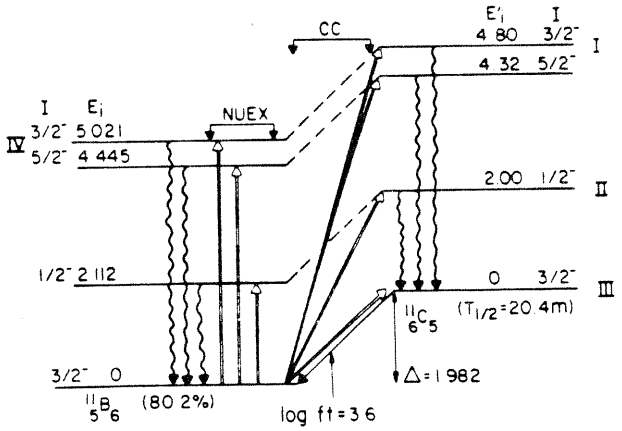

Fig. 1 Level scheme of $^{11}B-{}^{11}C$ system

2.2 All-flavor ν detection by Nuex: Another solar ν reaction on ^{11}B, based on the *neutral* weak current (NC), involves excitation of nuclear states (Nuex) in ^{11}B itself:

$$\nu + {}^{11}B \rightarrow \nu' + [\,{}^{11}B^*(E_i) \rightarrow \gamma(E_i) + {}^{11}B\,] \qquad (2)$$

This reaction operates *regardless of the flavor* of the incident neutrino. In ^{11}B, we will focus on Nuex transitions to a doublet of levels at E_i=4.45 and 5 MeV. In contrast to the broad bell-shaped CC spectra, Nuex events occur as sharp lines of energy E= 4.45 and 5 MeV for all $E_\nu > 4.45$ MeV, thus measuring the *total ν-flux created in the sun irrespective of any subsequent flavor transformations.*

2.3 Detection of Antineutrinos ($\overline{\nu}_e$): The Borex liquid scintillator will contain substantial amounts of H atoms. The presence of these free protons affords sensitivity to *antineutrinos* ($\overline{\nu}_e$) via the classic Reines inverse β^+ reaction:

$$\overline{\nu}_e + p \rightarrow n + \beta^+ \tag{3}$$

The neutron in (3) can be detected efficiently in Borex by the slow-neutron reaction:

$$n + {}^{10}B \rightarrow {}^{7}Li + \alpha + 0.48\ \text{MeV}\ \gamma \qquad (94\%) \tag{4}$$

Thus, a fast ($\sim$1 μsec) *delayed coincidence* of the β^+ in (3) with the 480 keV γ-ray of (4) provides a distinct signature. Since 20% of B occurs as ^{10}B and the cross section of reaction (4) is $\sim$4000 b, $\overline{\nu}_e$'s can be detected very efficiently, their energy spectrum being given directly by the spectrum of the prompt β^+ signal. Sensitivity to $\overline{\nu}_e$'s may be important because: 1) The Nuex signal integrates the ν as well as $\overline{\nu}$ flux. In order to compare it with the ν_e signal, the $\overline{\nu}_e$ contribution to the Nuex signal must be determined. 2) Recently, it has been pointed out[4] that a secondary flux of solar *antineutrinos* could arise from solar ν decay (into Majorons) following the MSW effect.

2.4 Electron-Neutrino Scattering: Another ν reaction not specific to B nuclei is that of (e$-\nu$) scattering on the electrons in the target:

$$\nu + e^- \rightarrow \nu + e^- \tag{5}$$

This is the basic reaction in Kamiokande-II (K-II),[5] where the highly forward-peaked distribution of scattered electrons is detected by the directionality of their Cerenkov emission. In the scintillation method, this cannot be used since the light emission is isotropic. The (e$-\nu$) signal could be as strong as that from (1) and its spectral profile is a monotonic decrease with energy, very different from that of (1).

2.5 Event Rates--Neutrino Signal from the Sun: In standard electro-weak theory, the excitation strength for Nuex, λ_{NX}, is directly related to the Gamow-Teller strength B(GT) of the mirror CC transition. For the ^{11}B$-^{11}$C isodoublet system,[1][2]

$$4\,\lambda_{NX} = \lambda_{CC}(\text{mirror}) = G_A^2\ B(GT)\ (\text{mirror}). \tag{6}$$

where $G_A = 1.26$ is the axial vector/vector coupling ratio. Preliminary B(GT) data for ^{11}B are now available from (p,n) reaction work,[6] calibrated by the known B(GT) for the ground state transition (CCIII). The λ_{NX} can also be derived from the relation[1]

$$\lambda_{NX} = 0.2963\ \kappa\ B_{ISV}(M1)\uparrow \tag{7}$$

where $B_{ISV}(M1)\uparrow$ is a matrix element derived from radiative data and $\kappa \approx 0.75$ allows for "quenching" of the weak relative to the γ strength. The λ_{NX} from (6) and (7) are in good agreement (see App. I for a complete discussion). Solar ν event rates for a standard model sun and ν's for the Nuex and CC transitions are given in Table 1.

Table 1. Solar Neutrino Yields (Standard Model[a]) for ^{11}B

NUEX($^{11}B \rightarrow {}^{11}B^*$)			CC($^{11}B \rightarrow {}^{11}C, {}^{11}C^*$)			(e−ν)
E (MeV)	λ^{b}_{NX}	Y^{b}_{NX}	E (MeV)	λ^{b}_{CC}	$Y^{c,d}_{CC}$	Y^{d} (TMBX)
			0	1.55	1744	
2.12	0.15	120	2.00	0.6	337	
4.45	0.21	72	4.32	0.84	166	
5.02	0.21	56	4.81	0.84	126	
Total NUEX (to 4.45+5.02)		128	Total CC		2373	1550

a) ^{8}B solar ν flux $\phi = 6x10^{6}/cm^{2}sec$; b) Average of radiative and (p,n) data;
c) Yield/200 Tonnes natural B/yr; d) Yield for total event energy E > 3.5 MeV.

The rate for (e−ν) scattering which depends on the electron density in the scintillator, can be calculated precisely in standard theory.[7] Fig. 2 shows the spectra of the ν reactions (eq. 1,2 and 5) in the case of the boron liquid TMBX (trimethoxyboroxine, see §4). The Nuex and (e−ν) spectra are shown on the left and the inverse β^- spectra on the right of Fig. 2. Besides the case of the standard sun and neutrino (bottom panel), profiles for two different cases of ν socillations in solar matter (MSW effect) are also displayed; note that the Nuex peak remains constant.

2.6 Antineutrino Signal from the Sun: The reaction (3) is well established.[8] Although no solar model predicts a measurable $\overline{\nu}_e$ flux, a *secondary* flux of solar $\overline{\nu}_e$'s is conceivable from ν decay into light pseudoscalars such as the Majoron (ϕ):[9]

$$\nu_2 \rightarrow \overline{\nu}_1 + \phi \qquad (8)$$

where ν_2 is a heavy mass eigenstate and ν_1 is a light one. In the theoretically preferred regime of small mixing and small ν mass differences, $\nu_e \approx \nu_1$ and thus the $\overline{\nu}_e$ should be practically stable, as confirmed by SN1987A $\overline{\nu}_e$ observations. However, the MSW effect in solar matter, operative in just this regime, can convert the initial ν_e into another ("heavier") flavor composed mostly of the *decaying* state ν_2 and thus *catalyze* ν decay.[4] Thus, despite small mixing angles, the MSW effect can not only create a resonant flavor conversion in the sun, it can also catalyze neutrino decay. This effect can create a strong secondary flux of solar $\overline{\nu}_e$'s. Fig. 3 shows the signal rate of reaction (3) as a function of the lifetime τ (governed by the ν-Majoron coupling constant g) for various lower cuts T^+ on the kinetic energy of the β^+ (3). In Borex, it may be possible to operate an energy cut as low as T^+=1.5 MeV. At this cut, the antineutrino energy $E_{\overline{\nu}_e}$ = (T^+ +1.8) MeV and the visible energy of the event is (T^+ +2x0.511) MeV. The present limits on g allow a large range of lifetimes for which the solar antineutrino signal is not only measurable but *larger* than the solar ν_e signal.

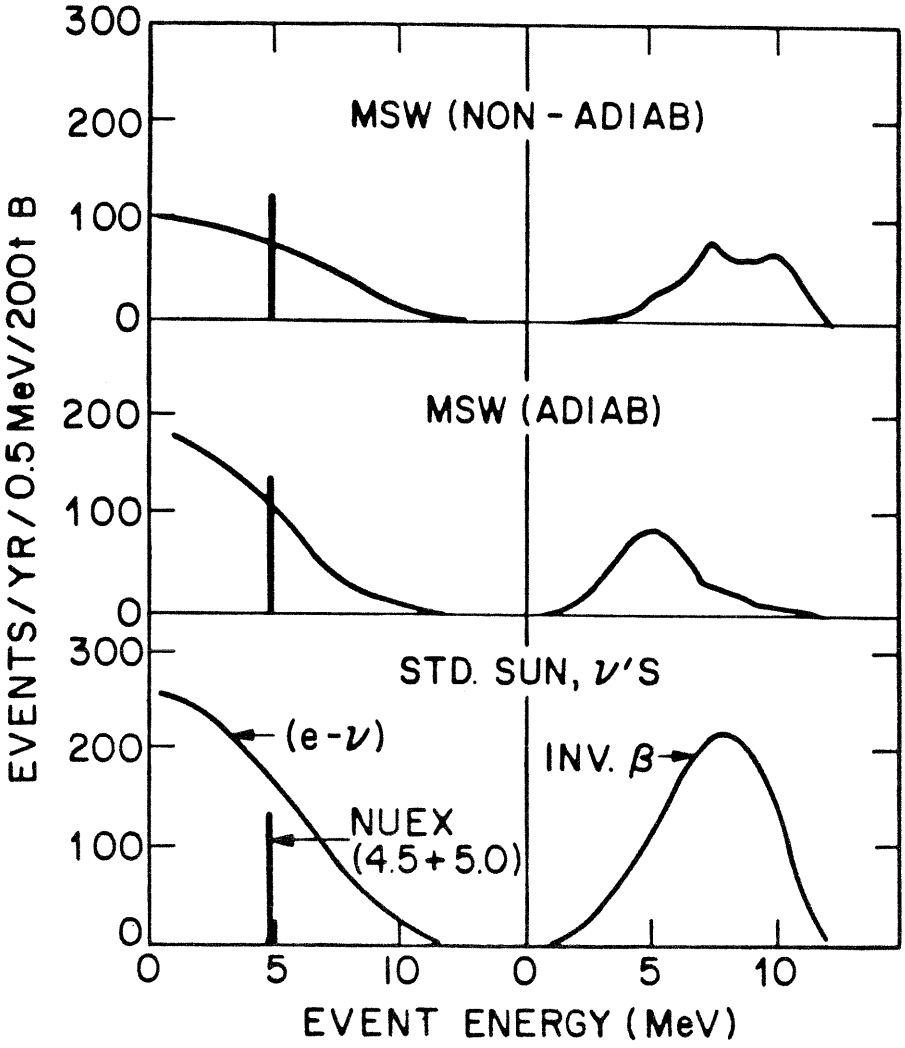

Fig. 2 Solar Neutrino Signal Profiles in Borex

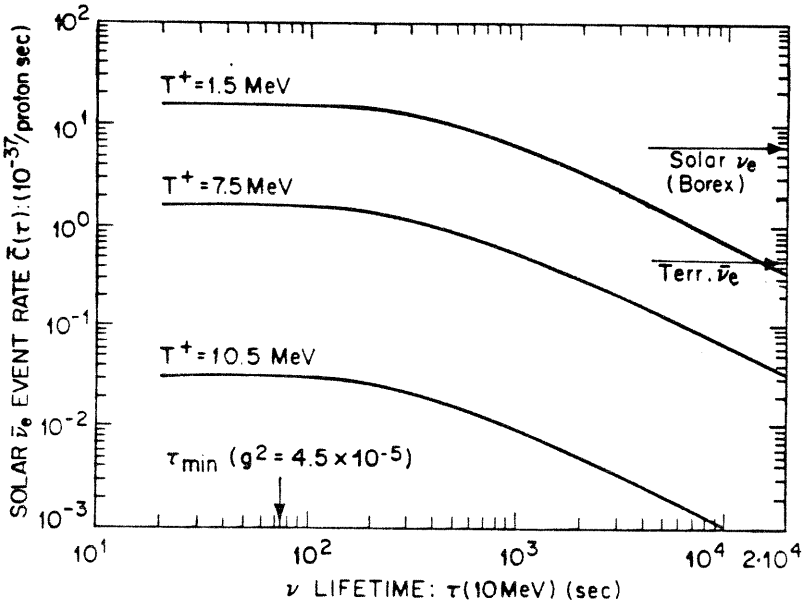

Fig. 3 Solar Antineutrino Signal due to MSW-Catalyzed ν Decay

3. Conceptual Design for Borex

The experimental approach best suited for low-energy work in Borex is *boron-loaded liquid scintillation spectroscopy, carried out in the style of the K-II or IMB nucleon-decay detectors.* An underground facility at a depth at least that of the Gran Sasso Laboratory (GSL) (Italy) assures an adequately low cosmic muon-induced background (see App. III). The external background and the B-content and density of the liquid scintillator dictate the proportions of the detector for a desired mass of B in the fiducial volume (FV). We have chosen trimethoxyboroxine (TMBX) (ρ=1.22g/cm^3)(§4), a liquid desirable from most points of view, as the detector medium.

The aim of the design is to suppress background from the radioactivity *external to the FV* of the detector to levels comparable to that from the only remaining unshielded source of radioactivity, the boron liquid in the FV itself. Other factors are: mechanical stability of the massive detector, maintenance of the chemical-, optical- and radiopurity of the scintillation liquid and total containment of the chemicals of the detector.

A spherical steel tank, immersed in a large pool of water in a barrel shaped cavern (Fig. 4) completely contains the TMBX scintillation detector, placed in a spherical inner vessel (IV) (14m dia., a few cm thick wall). The buffer space of 2.25m between the IV and the tank is filled with an inexpensive, transparent liquid (glycerol) with a density ($\rho\approx$1.2g/cm^3) matching that of the TMBX so that quiescent stresses on the IV walls are minimized. The IV is made of a transparent plastic that is chemically resistant to TMBX. Poly 4-methyl pentene-1 (TPX) is a possible choice. (Acrylic plastics are attacked by TMBX; they may be suitable only with a thin (<0.1mm), pin-hole free lining of transparent, TMBX-neutral film, e.g. teflon, nylon or polyxylylene). All these

Table 2. Specifications for Borex Conceptual Design

Cavity dimensions (Pool Vol.)	$\sim$24m d(max) x 24m h
Spherical Tank dimension	18.5m d
Spherical Inner Vessel (IV) dimension	14m d
Fiducial dimension	12.5m d
Tank volume	3315m^3
Buffer volume	1875m^3
IV volume	1440m^3
Fiducial volume	1020m^3
Total Scint. mass	1760 tonnes
Fiducial Boron mass	197 tonnes
Surface area of IV	615m^2
Number of PMT's (50cm dia.)	1450

plastics are normally made with the required radiopurity, <10ppt U/Th. Fig. 4 shows one method of supporting the IV using strong plastic cross-ribs anchored to the tank.

The scintillation light emerging from the IV is radially guided to the phototubes (PMT) fixed to the tank wall, by light pipes placed just outside the IV. These light pipes of a new design[10] are open-ended, hollow, barrel-shaped (see Fig. A4, App. V) plastic cylinders (78cm max. dia, 1.85m long) with a reflecting surface and held by a lattice anchored to the tank. The ambient liquid serves as the guide medium. The optics of these light pipes (treated in App. V) are such that: a) they provide a 180° field of view into the IV, even extreme rays from the inner shield being detected with ≤ 3 guide reflections; b) the light from the FV is observed with 0, 1 or 2 reflections, (nominal reflectivity 0.9); and c) their size can accommodate the use of 1450 PMT units (50 cm dia.)[5] within the geometry of the CD and the IV support structure of Fig. 4. The implies an effective PMT coverage of $\sim 30\%$, assuming $\sim 90\%$ transmission through the IV wall and 85% through the light pipe. Thus, these light pipes, while promising event sensitivity equivalent to direct detection, offer the important advantages of shielding between the PMT's and the IV as well as considerable freedom in the design of the mechanical support of the IV. "Blind" areas on the IV are permitted at the cross-rib supports of the IV and the light pipes can be configured for minimum interference with the cross-ribs and for maximum support area for the IV. Opaque materials (of high radiopurity) can be used for the support structure. In contrast, direct detection without light pipes requires 2350 PMT's for 30% coverage, assuming a fully clear IV. "Blind" areas will increase the PMT count besides creating complex shadows on the PMT's and posing ambiguities in the event reconstruction. A totally clear IV and its support impose severe restrictions on design and materials.

The steel tank shields the PMT's from the earth's magnetic field. For every event, the charge at each PMT which fires, the addresses of the fired PMT's and the timing sequence of the hits will be recorded so that the energy and spatial location of the event can be reconstructed *off-line,* taking into account various effects (such as bulk absorption and reflections in the light-guides) that depend on the location of the event. The key parameter for the spectroscopy and reconstruction is W=photoelectrons (pe)/MeV energy of the event. In Borex we expect W>100 PMT hits for a 1 MeV event and a signal threshold at ~ 110 keV (§4,5).

The active IV volume is divided electronically into a central fiducial volume (FV) and an "inner skin" which is the final, active filter of the residual external γ-ray flux. Events in the skin, though visible, occur close to the wall (and the light pipes) and produce a typically localized cluster of hits with charges of many pe's, a pattern unlikely for an event in the FV. They can thus be clearly identified and rejected. The total skin event rate, mostly close to the wall, is ~ 2/sec (§6); already at ~ 25cm from the FV, it is ~ 2000/day, below the rates due to the internal activity in the FV (§6).

Fig. 4 Conceptual Design of Borex

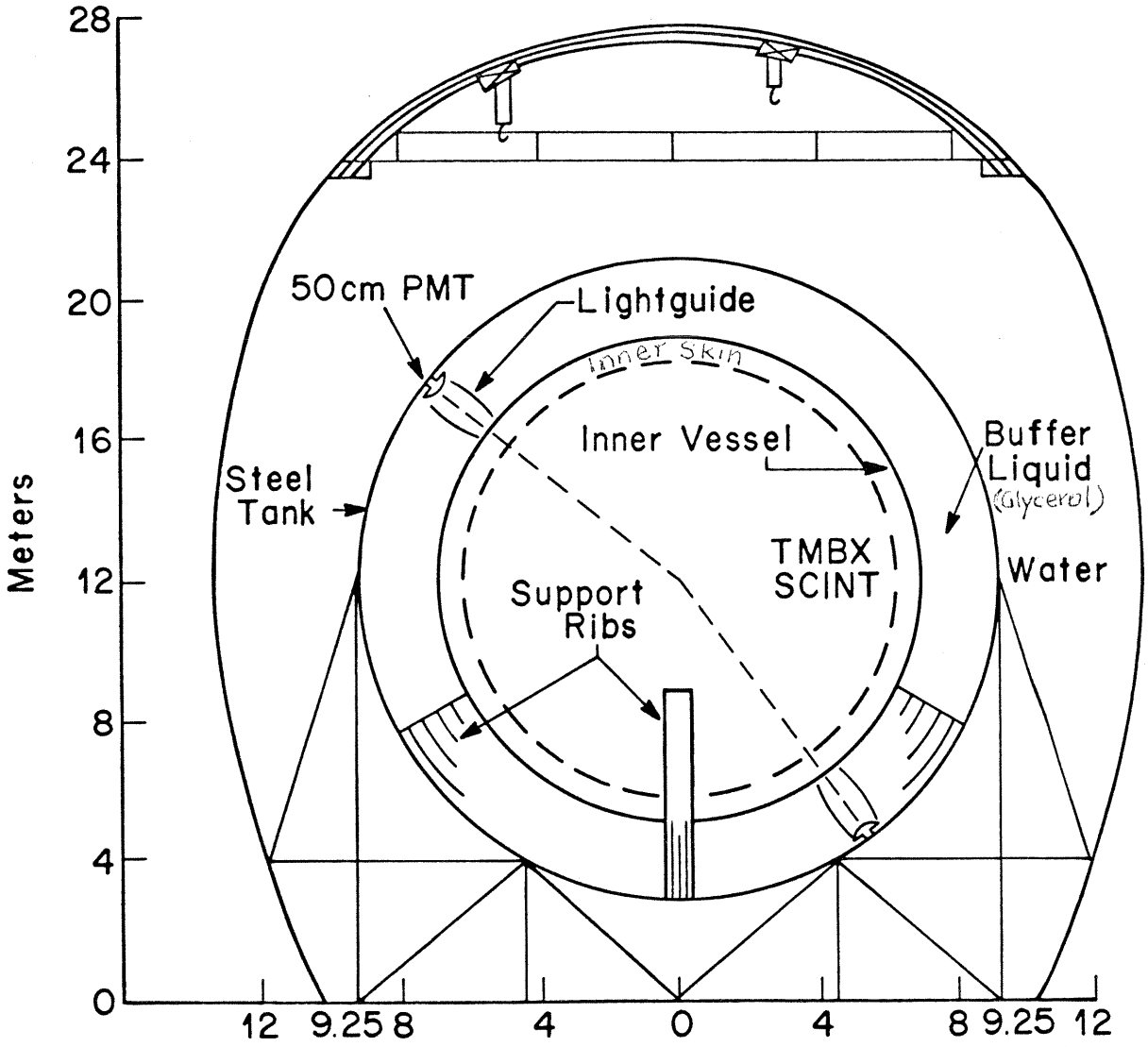

4. Boron Liquid Scintillators

4.1 TMB and TMBX--Photon Yields, Transparency: The central component of Borex is the boron liquid scintillator (BLS). The properties of prime interest are: the B-content, scintillation light yields and the bulk absorption of the scintillation light (since long light paths are involved). Two B reagents appear most suitable for Borex: TMB ($B(OCH_3)_3$; 10.5 wt% B) and TMBX ($B_3O_3(OCH_3)_3$; 18.75 wt% B). TMBX is derived from TMB by simple procedures. While the physical and chemical properties of TMBX are well known, (see Table 3) its optical characteristics, especially in the scintillation range, are not documented. As far as we know, the possible use of TMBX as a BLS reagent is suggested here for the first time. Its chemistry strongly suggests optical and LS properties very similar to those of TMB, described below. Optimization of TMBX as a Borex scintillant is a main part of current development.

BLS have been used routinely as slow-neutron detectors for many years. The standard mixture is TMB in solvents such as xylene, toluene etc.[11] Fig. 5 shows the variation of scintillation efficiency with TMB content in toluene and xylene solutions. Mixtures with 50% TMB retain 70-80% of the pure solvent light yields. The addition of naphthalene is found to increase the photon yield. Direct use of napthalene derivative solvents may be possible. The light yield of purified 1-methyl naphthalene (1MN) is among the highest observed in LS solvents.[12] Photon yields $\sim$40% of anthracene may be achievable in $\sim$85% mixtures of TMB (and hopefully, of TMBX) in 1MN.

Fig. 6 shows the (1/e) light attenuation length L in LS solvents in the uv-blue range of scintillations. TMB is far more transparent than most known LS reagents and, based on its similarity to methyl alcohol, L$>$20 m appears likely at 430 nm.

Table 3. TMB and TMBX: Chemical and Physical Properties

Property	TMB	TMBX
Formula	$B(OCH_3)_3$	$B_3O_3(OCH_3)_3$
Molecular Weight	103.92	173.6
Boron Content	10.3 wt. %	18.7 wt. %
Color and Form	Colorless Clear Liq.	Colorless Clear Liq.
Refractive Index (n_D)	1.366	1.4
Specific Gravity	0.926 (25 ° C)	1.22 (25 ° C)
Kinematic Viscosity	0.3 cs (25 ° C)	13.0 cs (25 ° C)
Melting Point	-29 ° C	10 ° C
Boiling Point	68.7 ° C	130 ° C (Decomp.)
Flash Point	28 ° C	35 ° C
Moisture Sensitivity	High	High

With such values of L for the TMB solute, absorption occurs mainly via the small 1MN component and the scintillation fluor. With the use of new fluors with large Stokes shifts such as PMP,[13] light attenutation lengths of L$\sim$10 m appear possible.

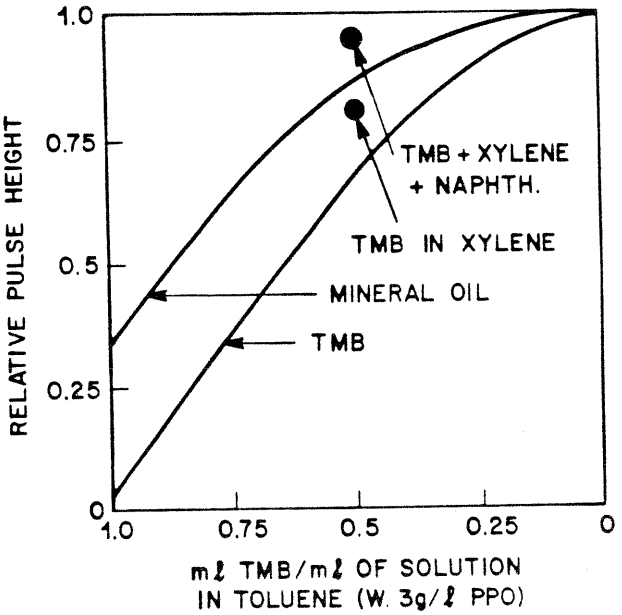

Fig.5. Light yields in TMB solutions (ref. 11)

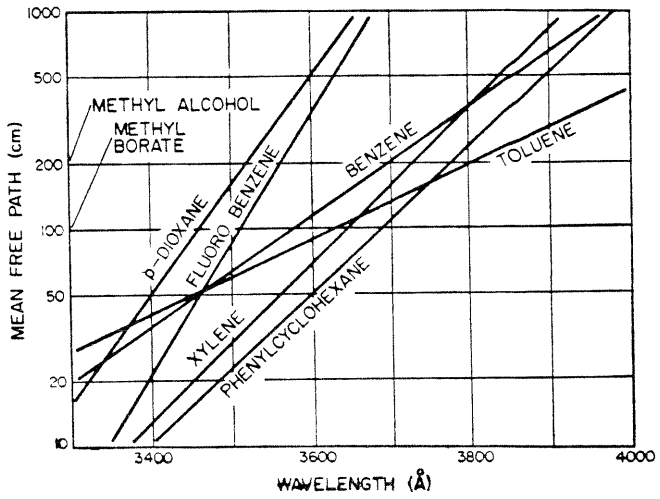

Fig.6. L vs. λ in LS solvents (ref. 11)

4.2 Manufacture of TMB and TMBX: The principal application of TMB is its use for making sodium borohydride for the paper industry. Thousands of tons/year are manufactured in the U.S. alone, the largest manufacturer being Ventron (Morton-Thiokol) Corp. The price of TMB is expected to be in range of $2500/ton.

The preparation of TMB is straightforward via esterification of boric acid:

$$B(OH)_3 + 3CH_3OH \rightarrow B(OCH_3)_3 + 3H_2O \qquad (9)$$

The TMB is separated by azeotropic distillation at low temperature (67 ° C). Several aspects of this process favor high radiopurity in the resulting TMB. The boric acid input material (from Mojave Desert, U.S. Borax) has been shown to be already very low in U/Th ($\sim 10^{-10}$g/g);[3] the methanol is made synthetically from gases; the process inherently involves distillation. The addition of another distillation stage with clean conditions (e.g. teflon-lined condensors etc.) can result in TMB of the radiopurity expected from laboratory distillation (see below) (§4.2) without demanding serious changes in the large-scale production process.

TMBX is made primarily for its use as a fire-retardant against metal fires. Most of it is now prepared by reacting B_2O_3 with TMB. This is probably unsuitable from radiopurity point of view because B_2O_3 is expected to be contaminated much more (orders of magnitude) than boric acid. However, an alternate procedure is available,

which may be appended directly to a TMB processing line. This involves the partial hydrolysis of TMB in presence of hexane and azeotropic distillation of the resulting hexane-methanol mixture:[14]

$$3B(OCH_3)_3 + H_2O + nC_6H_{14} \rightarrow B_3O_3(OCH_3)_3 + 6CH_3OH/C_6H_{14} \qquad (10)$$

This reaction is much more promising from radiopurity point of view since distilled TMB as well as highly refined hexane and purified water can be used. Production methods and the economics of this process are now under study. For a given B content, TMBX is expected to cost only marginally more than TMB.

4.3 TMBX and Operational Safety: Both TMB and TMBX have little toxic properties. They are moisture sensitive, even from air, thus requiring protected storage at all times. Shipping and large scale storage is done in tank cars with blankets of nitrogen gas. The boron liquid in Borex is maintained under nitrogen in the sealed-off inner vessel in any case, to minimize quenching of scintillation light by oxygen and other impurities. TMBX retards metal fires by creating, when ignited, a film of glassy molten boric oxide on the burning surface:

$$9O_2 + 2B_3O_3(OCH_3)_3 \rightarrow 3B_2O_3 + 6CO_2 + 9H_2O \qquad (11)$$

TMBX is classified as flammable. The geometry of the Borex CD may again be particularly helpful, since the TMBX will be completely contained in the sealed steel tank under $\sim$3 m of water. Also, the ambient water temperature in GSL is $\sim 10\,^{\circ}$C, well below its flashpoint. It is clear however, that thorough engineering studies must be conducted on these materials and, if necessary, additional features incorporated in the Borex design to ensure completely safe operation in an underground environment.

4.4 Radiopurity of BLS: The only unshielded source of background in the Borex CD is natural radioactivity in the fiducial BLS volume of the detector. The presence of trace U, Th and Ra in the BLS is of central importance for ν spectroscopy of events of energy E$<$5 MeV. For E$>$5 MeV, as in the case of the inverse β spectrum, radiopurity of the BLS is far less critical.

The radiopurity of boron compounds is being investigated at Bell Labs and preliminary results for commercial samples of boric acid (the starting material for the manufacture of TMB, TMBX) and TMB have been obtained.[3] The results for TMB are relevant also to TMBX since the latter is derived from TMB (§4.2)

The U/Th impurities in 12 l of TMB were concentrated by distillation of TMB. The residue was assayed by inductively coupled plasma (ICP) mass spectrometry at NRC, Ottawa. The contamination added by reagents used in collecting the residue was carefully measured in separate blank runs. Impurity contents of $<10^{-13}$g U/g and $\sim 10^{-12}$ g Th/g of commercial TMB were assayed, the sensitivity being limited mainly

by reagent contamination. Using TMB doped with known ppm amounts of U and applying the same procedures as above, mass spectrometric assay showed that the distillation process can decontaminate TMB of U by a factor of 1000. Similar measurements for Th are in progress. These results show that *TMB can be produced, at least on laboratory scale, with* $<10^{-16}$ *g U/g* (and probably 10^{-15}g Th/g) with one-stage distillation of the commercial TMB.

The investigations are being extended to TMBX samples as well as other components such as 1MN or pseudocumene in the BLS. In the case of TMBX, purification by other methods is necessary since it cannot be distilled. A promising method, now under development at Bell labs, is to use partial hydrolysis. Transuranic impurities present in the TMBX liquid scintillator will be in the form of organic compounds, most of which are readily hydrolyzed into compounds insoluble in the TMBX. A small fraction of a volume of TMBX will be hydrolyzed by the injection of water vapor under vigorous stirring of the TMBX. The created boric acid will precipitate and carry with it also the hydrolyzed U/Th compounds with it. Prior addition of Zr and Ba compounds to carry U, Th and Ra will also be tried. The precipitates will be separated by filtration or other methods. The purification efficiency of this procedure is expected to be at least ~ 10, which could lead to high levels of radiopurity by repeated hydrolysis. Since partial hydrolysis is the planned method for preparing the TMBX itself (see eqn. (10)), it is attractive to utilize the same method (with a filtration stage added) also for its purification.

4.5 Ultrasensitive methods for U/Th/Rn Determination: Solving the problem of radiopurity of the BLS entails the development of methods for *purification* as described above as well as those for *determination* of the transuranic impurity content. The impurity levels to be determined are in the range of 10^{-16}g/g. At present, no method of transuranic determination with sensitivity in this range is available; ICP mass spectrometry (U and Th) or fission fragment track etch (U) methods can reach 10^{-11} to 10^{-12}g/g. NBS has developed mass spectrometry for 10^{-14}g/g detection[15] which however, involves considerable prior processing of the sample and is not likely to be useful as a routinely applicable method. New methods are therefore necessary to improve the sensitivity to the desired levels, be simple enough for routine batch analysis of industrial lots of the BLS and to provide reliable data bearing directly on the actual counting levels in large volumes of the BLS. Several new ideas for achieving these results have been proposed (see App. VI), These are: 1) Isomer spectroscopy of activated nuclei (ISAN) for routine determination of 10^{-16}g/g of U and and Th[16] and 2) On-line counting of Radon in BLS liquids[17] for determining long-lived Ra out of equilibrium with U/Th.

5. Signal Sensitivities in Borex

5.1 Trigger Definition and Signal Thresholds: A valid event in Borex is a coincidence of n PMT hits out of a total of N, within a resolving time T. The PMT thresholds are set at $\sim$0.3pe level, creating a dark counting rate r in each PMT. The valid trigger n is so defined that the random n-fold coincidence rate from dark counts are below all signal rates in the detector. In the Borex CD, N=1450 and t$\approx$100 nsec (allowing for maximum photon flight times to the PMT's) and with PM's at $\sim$10 °C, r=2kHz (as at K-II)[18] so that NrT = 0.29. Then, thresholds in Borex are set by n = 11 for which the random trigger rate R is <70/year, most of which will be eliminated by tight tests on spatial reconstructability (see below).

The threshold sensitivities in Borex can now be estimated (Table 4) assuming that a photon efficiency 40% of anthracene is achieved in the BLS. In practice, the observed number of pe/MeV is smaller than that calculated using the rated quantum efficiency of the PMT. The "practical" efficiency factor, P, has been calibrated (using muons) to be 0.585 for K-II,[19] 0.53 for IMB[20] and 0.82 (using laboratory electrons).[21] We shall assume P=0.6. For events at the center of the detector (the most unfavorable position), the specific detection sensitivity is expected to be W = 100 pe/MeV. Since only a small fraction of the detector mass is at the center, the average is some 50% higher than this value. For a trigger threshold of n=11, the energy threshold should thus be at least *as low as 110 keV.* The figures at K-II are: W=2.2 hits/MeV and a threshold at $\sim$7 MeV.[5] Table 4 lists the threshold energies observable for particles of various types, taking into account the quenching of photon yields for heavier particles.[11] These sensitivities, typical of *radioactivity* physics, are tailored to tackle the fundamental background source in a solar ν experiment, viz. *radioactivity.*

Table 4. Signal Sensitivities Expected in Borex CD

Scintillation Photon Yield/MeV (S)	5500
Typical Absorption Loss in Scint. (A)	0.5
PMT Coverage (C)	0.3
PMT Quantum Efficiency (Q)	0.2
"Practical" Efficiency Factor (P)	0.6
Minimum Specific Sensitivity, pe/MeV (W= SACQP)	100
Threshold Energy (keV)	
β's, γ's	110
Protons	700
α-particles	2000

5.2 Detection Efficiencies: The low energy thresholds assure unit detection efficiencies (except for edge effects) of all relevant radiations. In particular, two low energy signals, the 480 keV γ-ray (in reaction (4)) and a 6.2 MeV α particle (of importance to the "Tl veto" (§6)), produce events with $\sim$50 and $\sim$60 pe. With a valid trigger at 11 hits, the γ-ray efficiency is determined only by edge effects. The chance of missing the α (no edge effects here) should be $<10^{-5}$.

5.3 Energy and Spatial Resolution: The energy of ionizing particles in Borex is totally absorbed and calorimetrically observed (except near the edges of the FV). The scintillation light produced by the event, measured by the total charge collected at the PMT's and the relative timing of the hit PMT's are recorded for every event. The total charge collected and the spatial distribution of the hit PMT's alone can provide a relatively fast, "on-line" reconstruction of the approximate energy and location of the event. Using both the charge and time information, an off-line analysis can fully take into account all the position dependent variables to yield a fairly precise reconstruction of the event in space, time and energy.

The performance of a typical configuration of Borex has been studied by Monte Carlo methods, using both the on-line (charge or pulse-height information only) and the full off-line (charge and time) reconstruction approaches.[22] In these studies Borex was assumed to be cylindrical (6.5m dia. and 16 m high), covered 30% by 50cm dia. PMT's, the specific photon energy/pe being 1500 eV as in Table 4. The energy was assumed to be deposited at a randomly chosen single-point, at least 20 cm from the wall. The light from each event is emitted isotropically and the amount of light on the PMT includes the solid angle intercepted by a flat area of the PMT and the bulk exponential absorption of the liquid (attenuation length λ). The refractive index which affects the light speed, was assumed to be 1.45. An overall timing jitter (1σ) of 4 nsec was assumed, which includes in quadrature, a single electron transit-time jitter (1σ) of the PMT (2.75 nsec),[23] and a scintillation lifetime of $\tau_s \sim 3$ nsec.

Unlike in K-II where the low Cerenkov efficiency results rarely in more than 1pe/PMT, multi-pe hits are common in Borex even at low energies. The analysis takes this into account by calculating the mean charge at each hit PMT by a Poisson distribution. Similarly, the mean time-jitter (τ_j^2) for a multi electron hit was scaled inversely as the number of pe's to simulate the improved timing in this case.

Fifty point events were generated and each analysed for 4 energies (1,2.6,5 and 10 MeV) and two values of λ (10 and 20m). The full off-line reconstruction finds values of R, the event location vector, energy E and the time t_o (the fit parameters) which maximizes the combined probability function $P_{tot} = P_{pe} \cdot P_t$ of the charge and time probabilities. The CERN program MINUIT was used. The resulting spreads ΔR and ΔE of the R and E fits, are given in Table 5 and Fig. 7a and 7b.

Table 5. Monte Carlo Results for Energy and Spatial Resolutions in Borex

Energy (MeV)	PMT's/event		pe's/event		Vertex Error (ΔR) 1σ (cm)		Energy Resln. (ΔE) FWHM (%)	
	λ=10m	20m	λ=10m	20m	λ=10m	20m	λ=10m	20m
1.0	110	150	160	200	16 (60*)	17 (46*)	28	20
2.6	250	330	420	560	10 (52*)	9 (32*)	12.7	11.8
5.0	390	520	860	1080	7 (45*)	5 (28*)	7.1	5.6
10.0	600	760	1680	2120	5 (42*)	4 (24*)	6.3	5.4

*Vertex error for "on-line" reconstruction based on pulseheight only.

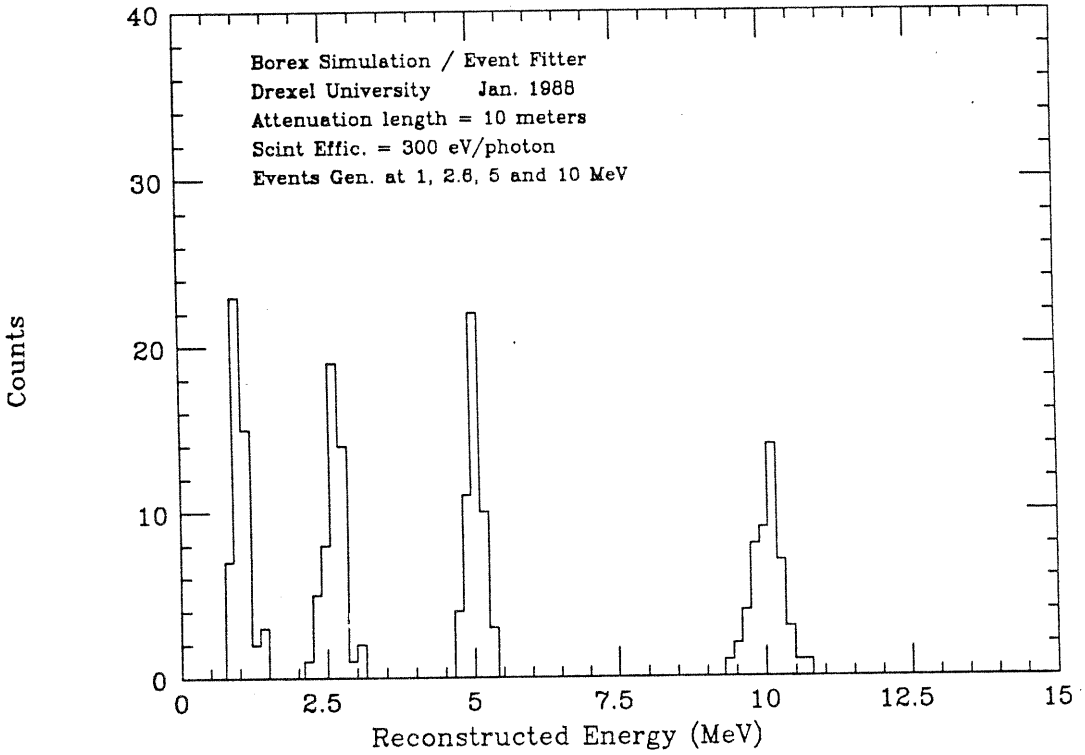

Fig. 7a. Energy Spread of Reconstructed Point Events in Borex.

The important role of the timing information in improving the detector resolutions is obvious from the data of Table 5. The spread in the fitted *time* t_o of the event was generally $\Delta t_o < 1$ nsec. Such a tight timing can reduce random events due to PMT noise to a great extent since it requires noise pulses to occur within a window

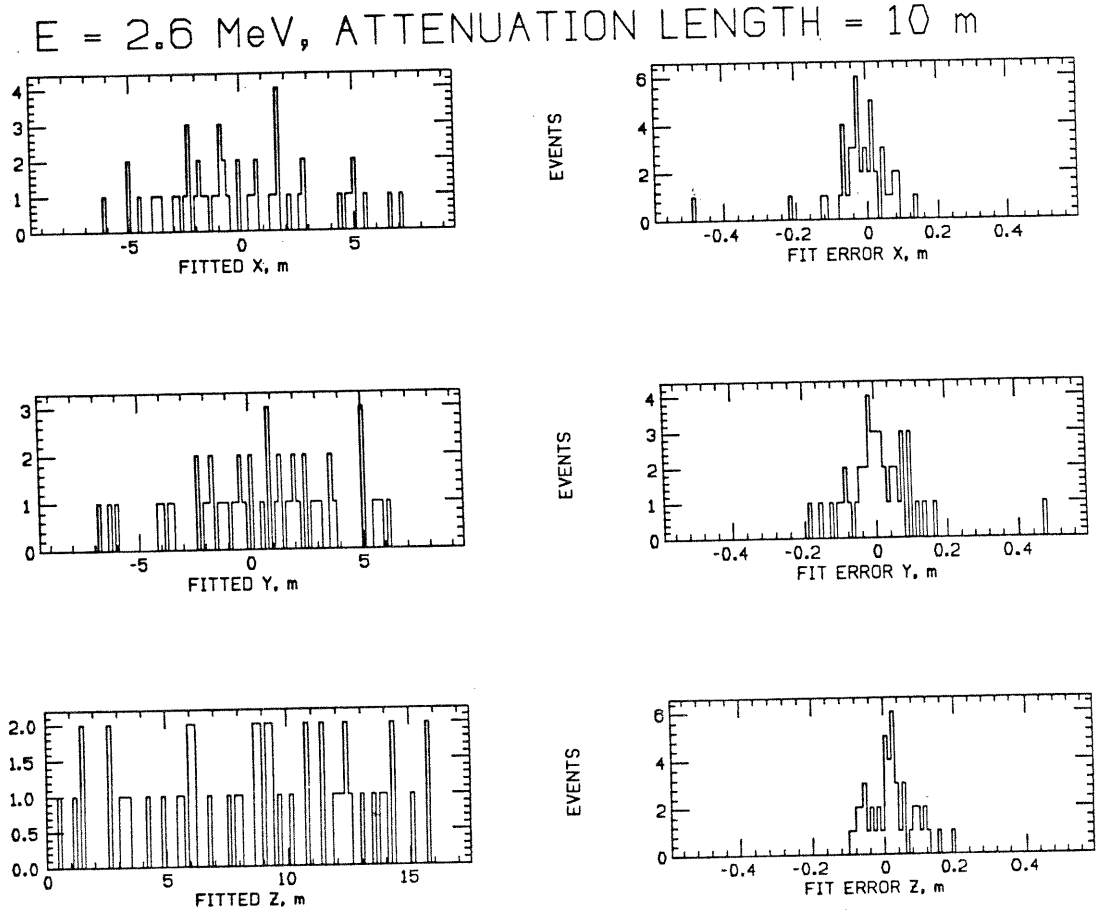

Fig. 7b. Spread in the Spatial Components of Reconstructed Point Events in Borex.

$<<$100 nsec for the event to be reconstructable. The above ΔR values, typically $\leq$7cm for E$>$5 MeV, may be compared to those observed at K-II, ΔR$\sim$1.7m for E$\sim$10MeV, showing that superior low energy spectroscopy is possible in Borex. The energy resolution is also of the class of table-top nuclear physics; e.g., a 5MeV event has a FWHM spread of only 360 keV.

Simulations of γ-ray showers are currently in progress. Although these events are spatially extended, the timing resolution is again of importance since the light from the major fragments of energy in the Compton shower (of a moderately energetic γ-ray) arrive at different times not only because of the different locations of these fragments but also because of the *delay due to the flight time of the γ-ray between Compton scatterings*. We expect that these two effects should provide timing patterns which are characteristically different from a point event of the same energy. For example, it may be expected that a 5 MeV Nuex γ-ray and a 5 MeV electron from an (e$-\nu$) event can be distinguished at least 90% of the time. The *energy* resolution of γ-ray events, in a full

reconstruction taking into account the timing effects, may thus be substantially the same as given in Table 5. We also expect that other types of events such as a through-going muon can be tracked into a cylinder of of radius ~ 5 cm because of the much higher levels of light production as well as the sharp signature provided by the entry and exit points of the track.

5.4 Pulse Shape/Particle Discrimination (PSD): Liquid scintillators including TMB mixtures, exhibit a sizable slow-decay component of the scintillation light from heavily ionizing particles such as p and α, commonly used to discriminate them from β's and γ's.[11] The typical lifetimes of the fast and slow components are 3 and 200 nsec. Since a major component of the background in the FV arises from the α's (~ 5 MeV), PSD against α's is of interest to Borex. Table 6 (ref. 11) shows relative strengths of the fast and slow components for 0.5 MeV β's and ~ 5 MeV α's producing equal signals.

Table 6. Pulse Time Discrimination of α particles in Borex

Particle	Signal (0-20 nsec)(hits)	Signal (0.2-1 μsec)(hits)
β's, γ's (0.5 MeV)	50	1.7
α's (5 MeV)	50	10

Table 6 shows that a candidate pulse of apparent energy 0.5 MeV produces, in the case of an α particle, a strong delayed signal, especially relative to the main pulse at short times. The chance of mistaking the delayed signal for that of a β is only a few percent. A dark noise generated delayed signal is only 2 hits for a dark rate of 2 kHz. The practicality of PSD vetoes of U/Th/Ra α's in Borex is thus clearly indicated.

6. Background in Borex CD

6.1 Background Sources and Shielding Architecture: *1) Radioactivity:* The general uncorrelated background in the FV of the detector plays a key role in the design of Borex. In the energy range of the solar ν signals it directly determines the S/N. In the lower energy regions it controls the effectiveness with which coincidence signatures for the signal (§7) and vetoes against background (§6) can be operated without risk of chance coincidences. In this section, a complete spectral profile of the uncorrelated background expected in the Borex CD is constructed. The profile is quantitative, but not based on computer simulations. It is, however, based to a large extent on measured data, using, when necessary, assumptions with margins of safety. To provide a design focus, we assume that the experiment is sited at GSL.

The sources of background considered here are all due to natural radioactivity, viz. the three important activities ^{238}U, ^{232}Th and ^{40}K. Thus the primary data base is a map of the distribution of these sources in the detector. This is given in Table 7. The U/Th levels cited here are either measured or typical. The data for GSL are from

Table 7. Distribution of Natural Radioactivity in Borex

Part	Mass (g)	U		Th		K	
		Conc.	Amt.(g)	Conc.	Amt.(g)	Conc.	Amt.(g)
Rock (GSL)		4.2×10^{-7}		6×10^{-7}			
Outer Skin (Water)	$\sim10^{10}$	10^{-11}	0.1	10^{-11}	0.1	10^{-7}	10^{3}
Steel Tank	1.7×10^{8}	10^{-8}	1.7	10^{-8}	1.7	10^{-6}	170
PMT's (#)	1450	4mg/PMT	5.8	4mg/PMT	5.8	0.7g/PMT	1015
Buffer Liq (total)	2.2×10^{9}	10^{-12}	22×10^{-4}	10^{-12}	22×10^{-4}	10^{-9}	2.2
-do- (<0.8m to IV)	7×10^{8}		7×10^{-4}		7×10^{-4}		0.7
Inner Vessel	1.5×10^{7}	10^{-11}	1.5×10^{-4}	10^{-11}	1.5×10^{-4}	10^{-9}	1.5×10^{-2}
Fiducial Volume	1.25×10^{9}	10^{-16}	1.25×10^{-7}	10^{-15}	1.25×10^{-6}	10^{-13}	1.25×10^{-4}

Bellotti et al[24] and those for the PMT's are from recent measurements.[21] The U/Th concentration in TMBX in the FV is indicated by preliminary laboratory tests;[3] for ^{40}K, however, the value is an estimate since no data on this are yet at hand. Values for the other components are based on typical data in the literature.

2) Shielding Dimensions: The FV is shielded from the radiations from the above sources by a graded arrangement of the CD. Table 8 summarizes the materials of the shieldings and their thicknesses as one approaches the FV from the rock wall.

Table 8. Shielding Dimensions in Borex CD

Part	Material	Thickness
Outer Skin	Water	2.75m
Boron Lining on Tank	Borated (5%) Plastic	0.05m (0.25g/cm^2 B)
Tank Wall	Steel	0.02m (0.16 mwe)
Buffer	Glycerol	2.25m (2.75 mwe)
-do-	(0.1%B)	(0.3gm/cm^2)
Inner Skin	TMBX	0.75m (0.91mwe)
Total (rock-FV)		6.57mwe
Total (Tank-FV)		3.66mwe
Total (PMT-FV)		3.15mwe

6.2 Low Energy Radiation in and into the FV: We can now construct a (theoretical) spectral profile of events due to unshielded local radioactivity and to γ-rays entering the FV from exterior sources. The result is shown in Fig.8. The continua are in units of events/0.5 MeV/day while the line features of energy E are plotted in the bin {E$-$0.5 to E} MeV in units of events/day. The energy resolution ΔE(E) (FWHM) is not folded in; ΔE(E) is, however, indicated at interesting spectral regions.

1) Local Background: Activities of U, Th and K traces in the FV produce a major part of the low-energy background in Borex, of which $\sim$75% are α events from U/Th. The events from local activities are of two classes: Nearly 60% of the α's are part of correlated sequences involving short-lived α activities of specific nuclides in the decay chain. These correlations can be identified and such events can be vetoed. The most important of these, involving the decay of ^{208}Tl, is discussed below; the rest are considered in App. II. The other class of events are due to uncorrelated radiations from α, β and γ events from U, Th and K isotopes in the FV. A composite spectrum of these events can be constructed from nuclear data on ^{40}K and the radionuclides in the ^{238}U and ^{232}Th decay chains (omitting those in Table A3, App. II). The spectrum is largely confined to $<$3.3 MeV (see Fig. 8), the end point of ^{214}Bi β^- decay. The total rate is dominated by α's (which appear with a signal equivalent of $\sim$ 0.5 MeV) at $\sim$ 1400/day (β's from ^{40}K at $\sim$700/day) falling off steeply with increasing energy.

2) The ^{208}Tl Background: The radiations of all but one of the natural radioactivities have a maximum energy of 3.3 MeV, significantly lower than the Nuex lines of 4.5 and 5 MeV. These background radiations can thus be tolerated at much higher rates than the Nuex signal. The exception is ^{208}Tl which decays (see Fig. 9) via $\beta+\gamma$ cascades with energies upto 5 MeV. Mimicking the Compton shower pattern of the Nuex γ-rays, they can tail into the Nuex signal. While the main defence against ^{208}Tl is a very low level of Th in the FV, it can be strongly aided by tagging the Tl radiations by the α's signifying the birth of ^{208}Tl. The "Tl veto" is a vital design concept for Borex.

^{208}Tl is formed by the α-decay of ^{212}Bi and decays in $T_{½}$=3.1 min by β^- emission (see Fig. 9). Since ^{208}Tl does not decay to the ground level of ^{208}Pb the emission consists of a continuous spectrum from 3.2 to 5.0 MeV. The specific activity of ^{208}Tl is $A \approx 1.2/day/10^{-8}$g Th. In Borex, with 10^{-15}g/g of Th in the TMBX, the number of Tl decays is $T \sim 150/day$, $\sim 25\%$ of which can appear with the Nuex energies. The Nuex signal (Table 1) is Nx= (0.2+0.16)=0.36/day, divided between the 4.5 and 5 MeV lines. We thus seek a rejection of the Tl events by a factor >100, which can be accomplished by tagging its *precursor* α (visible energy $\sim$0.62 MeV), occurring several minutes earlier in the same location.

Fig. 8 Estimated Profile of Uncorrelated Background in Borex CD

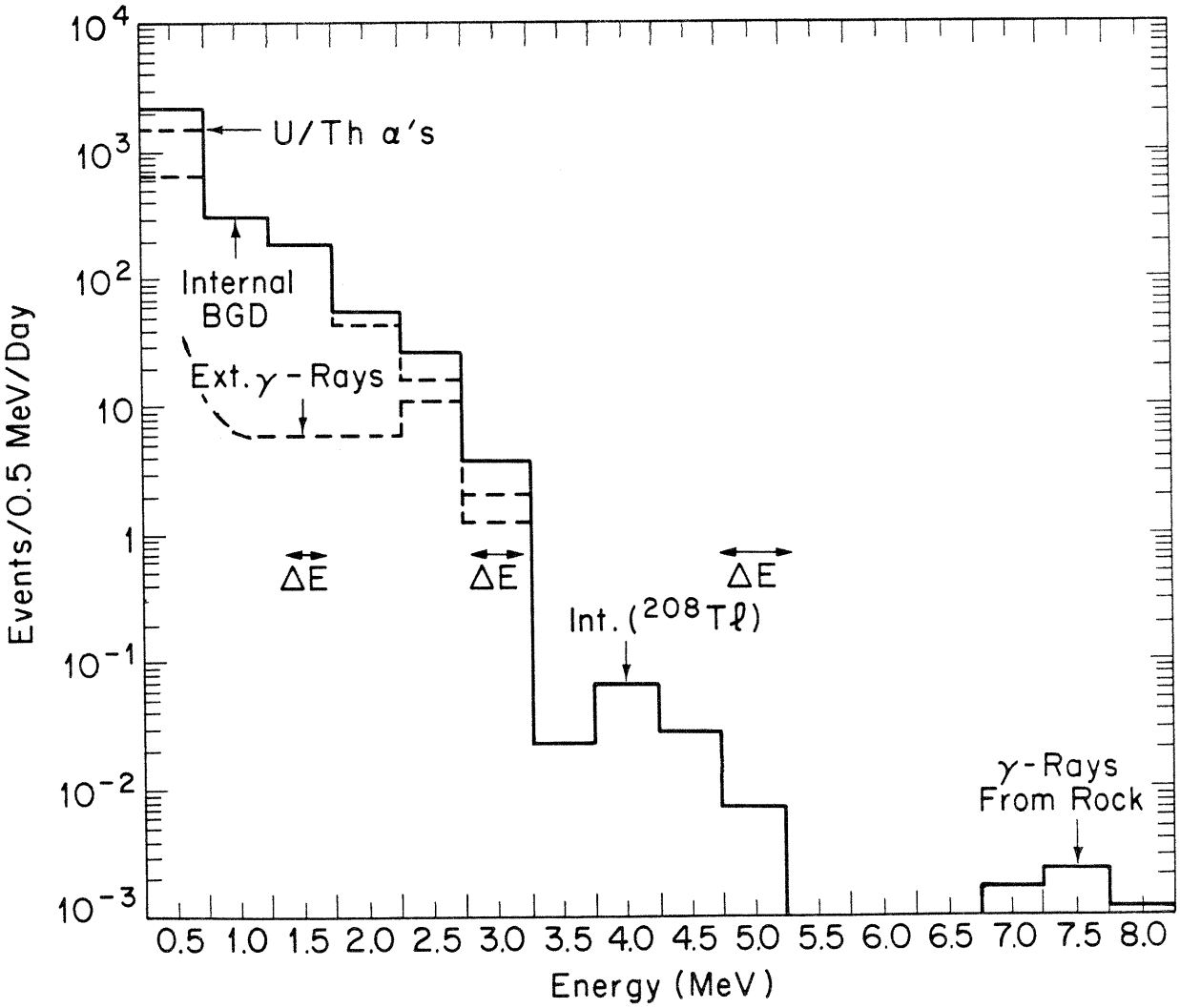

The Tl rejection efficiency is the overall detection efficiency (ϵ) of the precursor α ($1-\epsilon=0$; >62 hits vs. 11 trig.) in a gate-time of 13 half-lives of 40 min ($1-\epsilon=10^{-4}$). A spatial volume cut of $\Delta V=4m^3$ (radius 100cm, (4x 1σ ΔR), should result in at least $1-\epsilon<10^{-3}$ even for a distribution with a long tail. The Tl events can thus be rejected by at least a factor of 10^3, leading to the ratio Nx/Tl=2.4. However, some signal is lost because of false rejection of the Nuex signal due to a chance coincidence of a random *uncorrelated* α in the gates. The rate of α events is determined mainly by the U in the FV. If the U impurity level is at 10^{-16}g/g as indicated in laboratory tests, the uncorrelated α's occur at the rate of C$\sim$1500/day (see Fig. 8). With a time gate ΔT=0.028 day and $\Delta V/V = 4x10^{-3}$, the signal loss $\phi<20\%$. Thus, at the expense of 20% of the Nuex signal a 1000-fold rejection of the Tl events can be achieved with the detection sensitivities available in Borex. The spectral profiles resulting from this operation (see Fig. 9) show that the background directly under the Nuex peaks is then only $\sim$12% of the Nuex signal.

8) External Low Energy γ-rays: The γ-ray flux from sources outside the FV can be estimated using the distribution of the U/Th/K sources in the detector (see Table 7). Sources located at the rock wall generate low energy γ-rays from K and Th, e.g., a 2.61 MeV photon flux [24] of $\sim 6x10^8/m^2/d$. The attenuation of this flux is calculated assuming a parallel beam. For all other sources in the detector, we use a model in

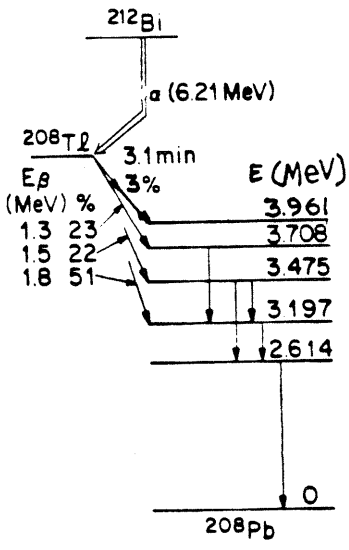

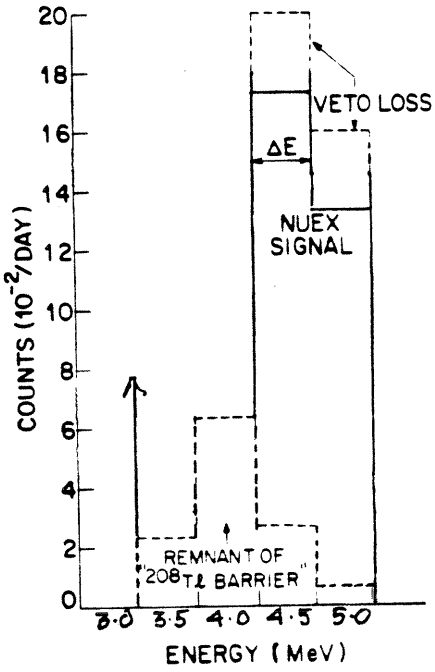

Fig. 9. $\alpha-\beta$ Correlated Decay of ^{208}Tl. Fig.10 The "^{208}Tl Barrier" vs. the Nuex Signal.

which these sources are assumed to be points. The γ-ray spectrum originating from these sources was constructed using nuclear data of the nuclides in the three sources. Then, the number of photons surviving after their passage across shielding matter (see Table 7) upto the IV without change in their energies, was calculated. Allowance is made for the fact that radiation from the point sources is divergent so that only a part of the original rays are close to the minimum path of the shield thickness. The rest traverse much longer paths and are liable to stronger attenuation. Finally, the "build-up radiation" due to the persistence of γ-rays scattered into lower energies[25] was accounted for by extending each surviving line into a flat spectrum with an intensity/bin equal to the intensity of the surviving line. This procedure should be reasonably correct except at very low energies ($\sim$200 keV) where the build-up intensity is seriously underestimated. This built-up spectrum arriving at the IV wall adds to the spectrum due to the sources in the wall and penetrates into the IV when all interactions become visible. The cumulative spectrum is attenuated further as the inner skin is traversed until the FV is reached. This final γ-ray spectrum is shown in Fig. 8. The upturn at low energies indicates the unestimated build-up at low energies.

The external low energy γ-ray spectrum in Fig. 8 arises 80% from the IV wall, 5% from the buffer liquid, 13% from the PMT's and 2% from other sources, mostly the tank. The spectrum is relatively flat, due mostly to build-up in the outer shielding, but the 2.6 MeV γ ray can be seen. The total counting rate due to the external flux in the inner skin is $\sim$2/sec, occurring mostly very close to the walls and decreasing rapidly as one approaches the FV. At a distance of $\sim$25cm from the FV (the nominal spatial resolution with which the FV boundary can be electronically defined), the counting rate is $<$2000/day, blending smoothly into the total rate in the FV due to local radiactivity. Notice that the external background (mostly due to the IV wall) is comparable to that of the internal one at around 3 MeV while at low energies it is insignificant. The CD thus achieves its aim of making the FV of Borex immune to background from external sources. *The low energy background in the FV is thus determined almost entirely by the radiopurity of the Boron scintillator.*

6.3 High Energy γ-rays: The main sources for these γ-rays are fission of ^{238}U and n-capture. We will consider capture γ-rays from the steel tank in the next section. The spontaneous fission of ^{238}U creates γ-rays at the rate of[26]

$$\frac{\mathrm{dN(E_\gamma \text{ in MeV})}}{\mathrm{dE_\gamma}} = 2000\,(\exp^{-1.05\mathrm{E_\gamma}})\ /0.5\mathrm{MeV/gU/day} \qquad (12)$$

The fission γ spectrum in the FV from the U distributed in the CD was calculated as before in the point source model. The γ-ray spectrum from the rock wall has been measured at Sudbury.[27] The spectrum at GSL was crudely estimated by scaling down the Sudbury γ-ray fluxes by a factor of 0.32 for the lower U concentration at GSL. The

attenuation of this flux was calculated simply in the parallel transport model. The result, as seen in Fig. 8 is a very small contribution at $\sim$7.5 MeV.

Table 9. Neutron Rates in Borex

Origin	U (g)	n/d(Start)	n/d(Out. Skin)	n/d(Buffer)	n/d(IV)
Rock (Slow n)		$4500/m^2$	17600	0.5	$\sim$0
Outer Skin	0.01	17.5	17.5	$\sim$0	$\sim$0
Steel	1.7	3000	1500	1500	0.004
PMT's	5.8	10000	5070	5070	0.01
Buffer Liq.	$2.2x10^{-3}$	5		5	$\sim$0
IV Wall	$1.5x10^{-4}$	0.26		0.13	0.13
IV (TMBX)	$1.75x10^{-7}$	$3x10^{-4}$			$3x10^{-4}$

6.4 Neutrons and Capture γ-rays: The sources listed in Table 7 also generate neutrons due to the spontaneous fission of ^{238}U as well as by (α n) reactions on light elements such as Na, Al in the rock, and on B in the FV. Neutron production in Borex is summarized in Table 9. The slow-n data at GSL (Lab. B) is from Bellotti;[24] it is higher than that at Sudbury[27] even though the U content of the rock (Table 7) is lower. Fission neutrons (fast-n) are produced at the rate of 1750 n/g U/day. Neutrons produced in the FV due to (α,n) is negligible, $5x10^{-3}$/day (see §7).

The principal target for n-capture and the resulting high energy γ-rays is the steel tank and the main source of neutrons is the rock. Thus, although the 2.5m water shield reduces the neutrons to $\sim$18000/d, additional shielding by a B layer on the steel is necessary. The half-thickness for n-capture in natural B is 16 mg/cm^2. Thus, a 5 cm layer of of 5% borated paraffin, coated carefully on the steel tank, will eliminate n-capture on steel. Neutrons produced in the buffer area (e.g. from the PMT's) can be similarly prevented from seeing the steel by doping the buffer liquid with B.

6.5 Other Sources of Background: An important consideration is cosmic muon-induced radioactivity, which dictates the minimum thickness of the overburden required for the experiment. As discussed in App. III, at shielding depths of the order of 4000 mwe (e.g., as in GSL), this problem does not pose serious interference in the operation of Borex. Other, less important sources of background treated in the App. II-IV are, background from α and neutron induced reactions on B in the FV, ν_e signals from materials other than ^{11}B and the non-solar antineutrino background.

7. Neutrino Reaction Signatures

7.1 Tags for ν-Reactions in Borex: The radiopurity of materials and the conceptual design of the detector are optimized so that the yields of solar ν reactions exceed background. Evidence of solar neutrino detection is provided (in the statistical sense), from the spectral shapes, assuming estimated background spectra. With the sensitivities available in Borex (§5), however, more *active* tests which can demonstrate specific ν origin of the events are possible. The facility of several ν reactions sensitive to different aspects of solar ν's can be fully exploited by using signature tags to sort out the various ν reactions and determine the reaction yields individually.

The four types of ν signals in Borex can be distinguished using: i) the nature of the spatial signal pattern of the ν-reaction product and ii) the appearance or absence of correlated events in temporal and spatial coincidence with the candidate event. Signatures based on these features (see Table 10) can tag specific reactions in Borex just as the (e$-\nu$) signal in K-II can be tagged by Cerenkov directionality.[5]

The inverse β reaction (1) results in the emission of a β^- particle which appears point-like. The reaction implies the formation of ^{11}C (Fig. 1) and its subsequent β^+ decay after a delay of $\Delta T \approx$ 21 min. with a maximum visible energy of 1.98 MeV. Thus the β^- from reaction (1) should be followed within $\sim\Delta T$ and within a coincidental spatial resolution volume ΔT, by a second event of energy (2x0.511) to 1.98 MeV.

Table 10. Tags for ν-Reactions in Borex

Reaction	Start event	E (MeV)	Profile	Pattern	Stop event	E (MeV)	ΔT	ΔV (m^3)
(ν_e, ^{11}B)	β^-	3$-$12	Bell Shape	Point	β^+	1$-$2	100 min	0.26
(ν_e, ^{11}B*)	$\beta^- + \gamma$	"	"	Extended	"	"	"	"
Nuex	γ	$\sim$5	Line	Extended	None			
(e$-\nu$)	e^-	4$-$10	Continuous $\downarrow$ with $\uparrow$ E	Point	None			
($\overline{\nu}_e$,p)	β^+	(1.5$-\sim$6) +1.02	Bell Shape	Extended	γ	0.48	10 μsec	4

The sequel appears not point-like but spatially extended because it consists of a β^+ and the showers from 2 annihilation γ-rays. For ν_e reactions to the *excited states* of ^{11}C, the initial β^- is accompanied by γ-ray of 2 or 5 MeV energy and thus presents an extended spatial pattern, enabling the separation of such transitions from the main ground state reaction. Such details provide proof for a ν-induced inverse-β reaction. In a similar

way, the ($\overline{\nu}_e$,p) reaction (4) can also be demonstrated by a tag based on time-correlated events but with a much shorter time-gate.

A candidate event with the precise energy of 4.5 or 5 MeV energy, in the *absence* of a correlated sequel, may imply a Nuex or an (e$-\nu$) event. The Nuex γ-ray shower is spatially extended over a typical radius of $\sim$25 cm while an (e$-\nu$) event appears point-like. They can thus be differentiated $\sim$80% of time (see §5). The sharp line feature of the separated signal at the predicted energy is the basic Nuex signature.

7.2 Background limits for Reaction Tags: In order to identify ν_e and $\overline{\nu}_e$ signals by delayed coincidence tags, in practice, the background rate in the volume ΔV must be limited to minimize chance coincidences in the relevant time-windows (ΔT). The ΔV is set by the spatial resolution. What are the limiting background rates?

I. The ν_e Tag--Reaction (1): Let us aim for a tagging efficiency ϵ=0.95 and the average fraction of false taggings arising from chance coincidences, $\phi<0.05$. ϵ is determined by the cuts on ΔT and ΔV. With a spatial resolution ΔR(1σ) of 20 cm for a β^+ of 1-2 MeV, 95% of the event-pairs will be reconstructed within a sphere of 40 cm radius, and a fractional resolution volume ΔV/V=2.7x10^{-4}. 97% of the ^{11}C decays will occur in ΔT=100 min=0.069 d so that, in effect, ϵ=0.95 can be satisfied. The demand $\phi<0.05$ is met if the rate/day at 1-2 MeV in the total FV, is C(1-2 MeV)$<$ 2700/day. The rate from Fig. 8 is $\sim$500/day, 5 times lower than the above limit on C. Observation of time-correlations over such durations should thus be practical in Borex, facilitating the signature for inverse-β events and separating them from the raw signal profile.

A different question is: Will the initially produced ^{11}C atom remain in the location (ΔV$\sim$1m^3) of its birth for this duration in order that the subsequent β^+ can be registered in spatial coincidence? Diffusion theory indicates that, under equilibrium conditions, it will require $>$1 month to displace the atom by 1 m in ordinary liquids. The dominant factor is, however, convection in the massive tank. A crude estimate of the velocities of convective mass flow has been attempted (by P.G.Simpkins, Bell Labs). assuming a cubical tank, 15 m on the side, containing liquid TMBX maintained at a temperature difference $\Delta\theta$ of a few degrees from the surrounding buffer liquid. The main conclusions are: Close to the walls, a boundary layer with high vertical flow velocities is formed. Maximum velocities of the order of a few cm/sec develop, but the thickness of this layer is only O(1cm). Flow velocities decay rapidly towards the interior; beyond $\sim$20 cm from the wall, the velocities are already $<$10cm/hour/$^\circ$ of $\Delta\theta$. The vertical flow reverses at the top of the tank into a central downflow plume. The thickness of the plume is small, O(1cm) and extends part of the way down the tank, generating circulation cells with small horizontal velocities in the upper portion of the tank.

Thus, in the Borex FV which is located at a distance of 75cm from the walls, the liquid transport is expected to be slow, $\sim$10 cm/hour. Thus, in the time-gate of $\sim$1 hr, the liquid displacement is likely to be less than the 40 cm radius assumed above for the volume cut for the inverse-beta delayed coincidence. Occasional instabilities with faster displacements may occur, but these "dead" fractions of the FV are likely to be less than the 5% loss assumed above for the efficiency ϵ of the delayed concidence. It would thus appear that convection in the tank may not interfere with the operation of signal signatures in Borex. However, because of the nature of the problem, practical tests are necessary to confirm these conclusions. Since the problem scales as $(\Delta\theta/\mathrm{h})^{-1/4}$, experiments on mass flows in tanks of smaller linear sizes h may reveal quantitative results relevant to the operation of Borex.

II. The $\overline{\nu}_e$ Tag--Reaction (4): The $(\overline{\nu}_e,\mathrm{p})$ reaction releases a neutron with tens of keV energy which diffuses in the hydrogenous BLS and is absorbed with high efficiency by a ^{10}B nucleus, present in the BLS to the extent of $\sim$3%. 94% of the n-captures result in the emission of a γ-ray of 0.48 MeV. The neutron diffusion time, typically $\sim$1 μsec provides the delay. The tag efficency ϵ is $\sim$1, since: a) the detection efficiency of the 0.48 γ is $\sim$1 (§5), and b) values of ΔT$\approx$ 10 μsec, much larger than the diffusion time and ΔX(3σ)$\sim$1 m can be selected. Random coincidences should be negligibly small because of the small ΔT. Background in this case arises mainly from $\overline{\nu}_e$'s emitted by nuclear power reactors in the vicinity (see App. IV).

8. Signal vs. Background in Borex

8.1 The Solar Neutrino Signal in Borex: The total background expected in Borex is confronted in Fig. 11 with the solar neutrino signals assuming standard models for the sun as well as the neutrino. The main features of the background profile are, a rapid decay upto 3 MeV where it is within an order of magnitude of the raw solar signal, and a much weaker tail upto 5 MeV. Above this energy the background is practically zero. In comparison, the total (raw) solar neutrino signal exceeds noise from $\sim$3.5 MeV, the signal/noise ratio increasing rapidly from a minimum of S/N=10 at 3.5 MeV to S/N$>$1000 above 5 MeV.

The shielding architecture of Borex and the radiopurity expected in the scintillator have been shown to result in background rates (at the relevant energies) well within the ranges required by the coincidence signatures (see §7) of the inverse β reactions. The signals of the three neutrino reactions can be successively sorted in off-line analysis as follows (§7): i) The inverse β events can be first separated (using the delayed coincidence) with $>$95% "purity" from other reaction signals at all energies; ii) The remainder is a "pure" (e$-\nu$) signal at all energies except at the Nuex lines. iii) The Nuex$-$(e$-\nu$) separation can be carried out by spatial pattern-recognition (point vs extended) $>$80% of the time. The raw total solar signal in Fig. 11 (solid line) can thus be unraveled into its components (drawn below it in dashed lines).

8.2 The Nuex Signal: The effect of the "pattern cut" in substantiating spectral line features at the precise Nuex energies (and nowhere else), is similar in importance and effectiveness as the "directionality cut" in Cerenkov spectroscopy as in K-II. In the raw signal, the ratio of the Nuex peak height to "valley" of scattering events is $\sim$0.4. in the "worst" case of no ν oscillations, as in Fig. 11. With a $\sim$80% discrimination of the extended (Nuex) events from the point (scattering) events, the peak/valley ratio should improve to a value of $\sim$2. In a year's livetime, the Nuex signal ($\sim$110 events) can be determined to some 15% precision even assuming the limited statistics of only the $\sim$65 (e$-\nu$) "background" events which survive the "pattern cut" immediately under the Nuex peaks. The subtraction of the (e$-\nu$) background can be made with much higher precision because the overall (e$-\nu$) profile, containing some 1500 events, can be determined much more accurately. The *non-*ν background under Nuex is $<$15% and does not worsen the final precision of the Nuex yield significantly.

The yield of Nuex signal, obtainable with some 15% precision in a year's livetime in Borex calibrates the total "all-flavor" neutrino output of the sun and provides a direct measure of the central temperature of the sun.

8.3 Inverse β Signal: The facility of the delayed coincidence tag enables not only the separation of the inverse β signal from the other types of solar ν signals, it allows its

detection down to low energies $\sim$3 MeV. With the parameters used in §7.2, we can see that the coincidence tag can detect inverse β signals with S/N$\sim$1 even if the raw counting rates are $\sim$50 times larger than the signal, a situation that holds at the 3 MeV bin. Thus the useful spectral span of the inverse β signal is $E_\beta > 3$ MeV, with a total yield of $\sim$2300/yr. Through most of this range, the background should be vanishingly small.

After separation from the main signal by the delayed coincidence tag, the total inverse β yield contains, in addition to the transition to the ground state of ^{11}C, also those to the excited states. The latter, which amount to $\sim$25%, are accompanied by γ-rays (see Fig. 1). Thus, the excited state transitions can be resolved by further applying the "pattern cut" as in the case of the Nuex-(e$-\nu$) separation. The inverse β yield to the 5 MeV doublet is fundamentally related to that of Nuex yield from the mirror doublet in ^{11}B, as stated by eq. (6). This relation assumes that the neutrino flux at the detector is composed *entirely of electron neutrinos.* The ratio is thus a crucial and direct test of the *conservation of ν flavor,* and thus of the presence of ν oscillations.

The *nature* of the ν oscillation can be followed up by the *spectral shape* of the strong ground state inverse β transition which sensitively reflects resonant ν oscillations in solar matter. The shape distortions being directly controlled by the ν mass-differences and flavor-mixing angle, the more sensitively small distortions are detected, the more far-ranging is the search for new neutrino physics. From this point of view, a particular advantage in Borex is the *low* lower bound of $\sim$3 MeV, exposing nearly the complete bell-shape of the inverse β spectrum. In the absence of *resonant* ν oscillations, this shape is a pure "statistical shape" (eq. A2) which can be tested by Kurie-type analysis used in standard β decay since the initial ν spectrum due to the β^- decay of ^{8}B in the sun is precisely calculable. Such a test can sensitively demonstrate small spectral distortions provided, data is available at *low energies.* Thus the MSW effect can be sensitively tested over a large map of the relevant parameters. In comparison, Cerenkov methods such as that at K-II become marginal below 6 MeV, thus losing the crucial lower half of the bell-shaped inverse β spectrum. In this case, conclusions on the small shape changes can be misleading.

8.4 The (e$-\nu$) Signal: The final component is the substantial (e$-\nu$) scattering signal, amounting to yield of 1500/year. Its yield and shape depends on both *neutral and charged* currents. This data is thus a valuable confirming check on the overall correctness of the conclusions drawn from the Nuex and inverse β signals.

Fig. 11 Solar Neutrino Signal and Background in Borex-I

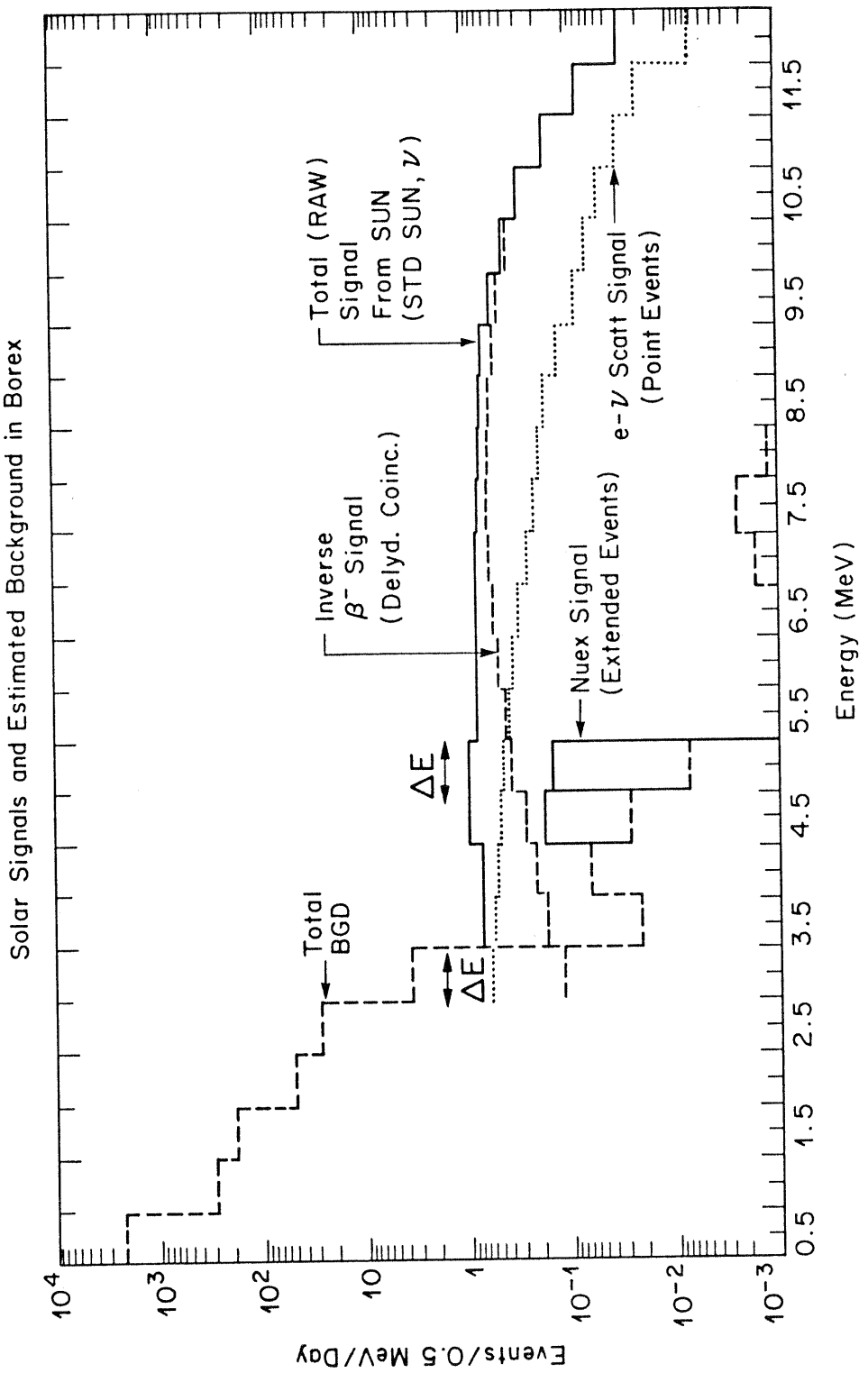

Conclusions

The discussions given in this report show that the operation of Borex can be based on a reasonably robust design framework. Its main strengths are: First, a well-demonstrated detection technique and the adaptability of boron liquids to high-quality liquid scintillation work are at the heart of the design. Secondly, the high signal sensitivities possible in this approach facilitate the operation of key design elements such as the signatures and vetoes, complementing the unique nuclear features of ^{11}B. Thirdly, the single most critical parameter, the required radiopurity of the boron liquids, may be in the attainable range. Finally, the availability of the massive amounts of boron materials underscores the practicality of the project.

In the present development phase of Borex, the following investigations assume a degree of priority: (1) Optimization of the optical and scintillation properties of TMBX. (2) Investigations on the control of radiopurity of the TMBX scintillator from manufacture to measurement. (3) Extensive monte-carlo simulation of the background profiles and the various signature and veto operations.

Three of the four possible detection modes in Borex, the $(\nu_e, ^{11}B)\beta^-$, the $(\overline{\nu}_e, p)$ and the $(e-\nu)$ scattering modes can be observed even with presently available TMB scintillators despite the lower boron content. Delayed coincidence signatures available for the first two, allow several facilities: the reaction modes can be separated from one another; the question of radiopurity becomes less critical and a spectral range with a low lower bound becomes accessible. A spectrum certified as due to $(\nu_e, ^{11}B)\beta$, for example, can be recorded with a quality ratio of S/N$>$10 for β energies $>$3 MeV. These minimum expectations from Borex already exceed goals projected for other approaches in terms of signature, low energy sensitivity and types of ν modes.

On the other hand, observation of the Nuex signal with a good S/N depends on the reasonable expectation that the preliminary results from radiopurity tests are realized in field practice, in which case, it will be possible to attain the full physics potential of Borex, viz.,

- A measurement of the Nuex signal to a precision of $\sim$15%, calibrating the ^{8}B ν output of the sun and revealing the astrophysical structure of its central core. Relative to this calibration, new properties of the ν can be investigated via the inverse β signal.

- A fairly precise determination of the shape of the inverse β spectrum. With the signal statistics and the spectral range accessible to Borex, especially at low energies, even small shape distortions indicating the presence of the MSW effect can be detected.

- Confirmation of such ν effects by the yield and shape of the $(e-\nu)$ signal.

New findings in ν physics can be cross-tested in Borex by four different observables, the (Nuex/CC) signal ratio, the inverse β spectral shape, the (e$-\nu$) signal and the flux and spectrum of solar antineutrinos. As shown in the analyses of ref. 2 and 4, using these cross-tests, it may be possible to make a definitive probe of the subtle nature of the neutrino despite the welter of non-standard ν scenarios proposed so far.

Acknowledgements

This work has benefited from generous help from and valuable discussions with many individuals. We wish to specifically thank: Sandip Pakvasa, Xiao-Gang He and B. Alec Brown for their theoretical contributions; Martin Deutsch for many helpful discussions and Walter L. Brown for his encouragement.

Appendix I: Neutrino Cross Sections

1) Event Rates: The solar ν event rates for NUEX and CC modes in the Boron experiment are given by:
(a) NUEX transitions:

$$Y_{NX} = \frac{G_F^2}{\pi} \phi \lambda_{NX} P_{NX}$$

$$Y_{NX} = 1.68\text{x}10^{-44} \phi \lambda_{NX} P_{NX}/^{11}\text{B nucleus/sec} \quad \text{(A1)}$$

where:
ϕ = Solar ν flux = $6.0\text{x}10^6/\text{cm}^2\text{sec}$;
λ_{NX} = NUEX strength = $\frac{1}{4}g_A^2 <\sigma\tau_z>^2$; $g_A = 1.26$
P_{NX} = phase space factor = $\int S(E_\nu)(E_\nu - E_{threshold})^2 dE_\nu$
with $S(E_\nu)$, the incident ν spectral profile; Energies in MeV.

(b) Charged Current (Inverse-beta) Transitions:

$$Y_{CC} = 1.68\text{x}10^{-44} \phi \lambda_{CC} P_{CC}/^{11}\text{B nucleus/sec} \quad \text{(A2)}$$

where:
λ_{CC} = CC strength = $g_A^2 <\sigma\tau_->^2 = g_A^2 B(GT)$
$P_{CC} = \int S(E_\nu)\, W_e\, p_e\, F(Z,W_e)\, dE_\nu$
with $W_e = (E_\nu - E_{thresh} + 0.511)$; $p_e = \sqrt{W_e^2 - 0.511^2}$; Energies in MeV.
$F(Z,W_e)$ is the Fermi function (Z=6).

2) Relation between λ_{NX} and λ_{CC}: The boron system is an isodoublet mirror pair (T = 1/2). Within this doublet, the operators of the transitions from the ^{11}B ground state to an excited state (NUEX) and the inverse beta to the corresponding excited mirror level in ^{11}C are related as:

$$<\sigma\tau_z>^2 = <\sigma\tau_->^2 \qquad (T=1/2)$$

Thus from the definitions of λ_{NX} and λ_{CC} the following relation holds:

$$4\,\lambda_{NX} = \lambda_{CC} = g_A^2\, B_{GT} \quad \text{(A3)}$$

3) How to get λ_{CC} and λ_{NX}: *a) Charged Current λ_{CC}:* For the ground state transition ^{11}B–^{11}C, the ft value is known: log ft = 3.6. Thus, λ_{CC} is given by:

$$\lambda_{CC} = B(F) + g_A^2 B(GT) = 6165/4000 = 1.55 \quad \text{(A4)}$$

where 6165 is ft for $\lambda_{CC} = 1$ (superallowed 0-0 decay), B(F) is the Fermi and B(GT) the Gamov-Teller matrix elements. For this ground state mirror pair: B(F) = 2T = 1;

Therefore, B(GT) = 0.345(8)[28] For the excited states, B(F) = 0. (For 2.0 and 4.3 MeV levels in ^{11}C, B(F) = 0; for 4.8 MeV level, B(F)$\approx$0 within 5%). Thus they proceed only by B(GT). The B(GT) values have been determined by Taddeucci et al[6] at the Indiana Cyclotron using (p,n) reactions on ^{11}B at 0° with 160 and 200 MeV protons. Two kinds of measurements were made; 1) differential cross sections, and 2) spin transfer by polarization measurement. These two parameters were measured for the ground and excited states in ^{11}C. They are proportional to B(GT). Since the B(GT) for the ground state transition is known (see above), the relative and absolute B(GT) of the CC transitions to the excited states can be evaluated from these results. The self calibration makes this a reliable measurement. In addition, both the differential cross section and polarization measurements agree within 10% which is the order of the uncertainty of these determinations. The results are given in Table A1.

Table A1. Charged Current Matrix Elements from (p,n)

State in ^{11}C	$B(GT)_{exp}$	λ_{CC}
0	0.345(8)	0.548+1.0
2.0	0.40(4)	0.635
4.32+4.8	0.955(90)	1.52

It is worth stressing that for ^{11}B the B(GT) values are based on *relative* measurements in the same target and the states of interest are well resolved from each other and from the ground state. The general opinion that B(GT) values from (p,n) reaction are not completely reliable holds only for those cases where *no internal calibration is available.* This does not apply here.

b) Neutral Current λ_{NX}*:* Since λ_{CC} is known, relation (3) can be directly used to get λ_{NX} for the excited states, in particular to the (4.45+5.0) MeV doublet in ^{11}B.

4) Derivation of λ_{NX} from Radiative Data: The λ_{NX} for the excited states in ^{11}B can also be obtained from the *measured radiative widths* of these levels. For our earlier paper (P.R.L 57, 1801 (1986) the (p,n) results were not yet available and we calculated λ_{NX} by this method and obtained λ_{CC} using eqn. (3). Now these calculations serve as a check of the applicability of eqn. (3) for mirror pairs and also as a reverse consistency check of the (p,n) results. The radiative widths for ^{11}B have been measured by (e,e') scattering or resonance fluorescence (γ,γ').[29] yield the widths Γ_o and thus the reduced M1 strength B(M1) for decay to the ground state. The excitation strength, B(M1)$\uparrow$, is then known by using the spin statistical factors. It can be shown that:

$$\lambda_{NX} = \frac{1}{4} g_A^2 <\sigma\tau_z>^2 = g_A^2 \frac{4\pi}{3} \frac{1}{(\mu_n - \mu_p)^2} B_{ISV}M1\uparrow \qquad (A5)$$

where $B_{ISV}M1\uparrow$ is the isovector M1 spin excitation strength. We derived $B_{ISV}M1\uparrow$ from the measured $B(M1)\uparrow$ as follows: A theoretical calculation of the $B(M1)\uparrow$ values of the excited states was made with a shell model code which gave values in reasonable agreement with the measured $B(M1)\uparrow$. Then the isovector spin part of the M1 strength was calculated with the same wavefunctions. The ratio of the two theoretical values provided a factor for each excited state. This factor was applied to the *measured* $B(M1)\uparrow$'s and taken as the values for $B_{ISV}M1\uparrow$. Next, this was used in eqn. (5) to derive an "uncorrected" λ_{NX}. It is well known that the $B_{ISV}M1\uparrow$ and the B(GT) differ in their "quenching" by about 25%. Systematics show[30] that this difference is nearly uniform over many nuclear levels in this region. Thus we obtained the "corrected" λ_{NX} by multiplying the "uncorrected" one by 0.75. The λ_{NX} so obtained are compared in Table A2 with those derived from the B(GT) values from (p,n).

Table A2. Neutral Current Matrix Elements

State (^{11}B)	$B(M1)\uparrow$ (Exp)	$B(M1)\uparrow$ (Th)	$B_{ISV}(M1)\uparrow$ (Th)	$B_{ISV}(M1)\uparrow$ ("exp")	λ_{NX} [B(M1)]	λ_{NX} (p,n)
2.12	0.575(45)	0.868	0.950	0.63(5)	0.142(10)	0.159(16)
4.45	0.900(90)	0.785	0.896	1.03(10)	0.231(23)	
5.02	1.25(5)	1.124	0.915	1.02(4)	0.231(10)	
Doublet					0.46(3)	0.38(4)

The experimental (p,n) spectral shapes for the doublet[6] appear unresolved (see Fig. A1) but *symmetrical* at the two different resolving powers, supporting the equality of the λ_{NX} predicted above. The agreement of the two sets of λ_{NX} and thus the mutual confirmation of the two widely different methods is satisfactory. Solar neutrino rates in Table 1. are therefore calculated with the mean of the radiative and (p,n) values.

5) Further Studies on ν Cross-sections: In principle, two more experiments can throw additional light on the ν matrix elements. The first is the possibility of Nuex in the laboratory using LMPF neutrinos. Neutral current events can be observed with ν_e as well as ν_μ. Charged current events can be observed with ν_e. The higher energies and mixtures of ν flavors in the LAMPF ν beam imply some contribution due to matrix elements of higher order than those contributing at small momentum transfers as in the solar case. However, the Nuex/CC *ratio* should be nearly insensitive to these nuclear physics uncertainties. Since Borex operation depends only this *ratio,* a calibration of

the ratio by LMBF ν beams can be performed, if necessary, and minimize any uncertainties on the nuclear matrix elements. A Borex unit much smaller than the solar detector can be used in these experiments because of the high ν energies and fluxes. Besides being useful to the full-scale solar program, such a test experiment at LAMPF would be of intrinsic value to clarify the role of neutral current interactions in nuclear physics, complementing the long-standing investigations on parity violation in nuclear states.[31]

The second experiment is the measurement of the radiative *lifetimes* of the 2.0, 4.3 and 4.8 MeV levels in ^{11}C. These lifetimes are determined by B(M1) values which are related to the B(GT) values arrived at by the (p,n) results in exactly the same way that the B(M1) values from lifetimes of the *mirror* levels in ^{11}B are related to it. Since this relation involves the quenching factor, this result can explicitly determine this factor and place the ν matrix elements in the ^{11}B – ^{11}C system on a completely experimental basis.

Fig. A1 Neutron spectra from ^{11}B(p,n)^{11}C (E_p=200MeV) (From ref. 6).

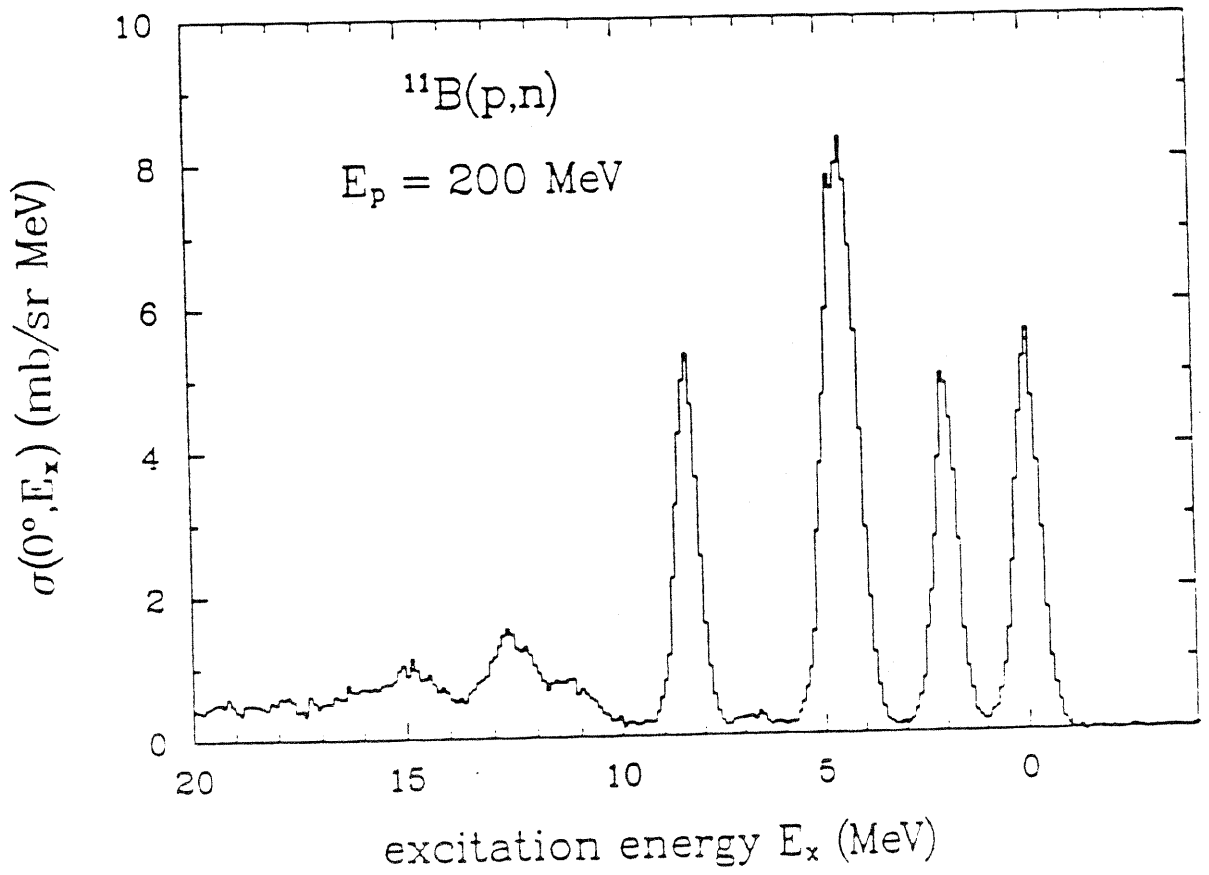

Appendix II. Correlated Events I: Internal Background

1) Correlated α Events in U/Th Series Decay: Activities of U and Th traces in the FV produce a major part of the low-energy background in Borex. Of this part, $\sim$75% are α events. Nearly 60% of the α's are correlated pairs arising from short-lived α decay of specific nuclides in the decay chain (see Table A3). The α's, though of several MeV energy, are visible only with typically a tenth of their energies and with spatial resolutions of $\Delta X(1\sigma)<15$ cm, but specifically identifiable by the PSD facility (§5). The time-gates of the correlations range from μsecs to minutes. Detecting these correlations is valuable because they provide a direct sampling at various points of the two decay chains, test for secular disequilibrium (thus for the presence of Ra) and in general, offer a sensitive tool for deriving *in vivo,* a precise make-up of the internal background in the FV. The conditions on the background counting rates for operating these tags are less restrictive than the Tl veto (§6) because of the generally shorter time gates.

Table A3. Correlated Events from U/Th Activity in FV

	Source	Start event	E (MeV)	Pattern	Stop event	E (MeV)	Pattern	$\Delta T_{1/2}$
1	^{222}Rn	α	5.6/10	Point	α	6.1/10	Point	3.05 min
2	^{214}Bi	$\beta^- + \gamma$	0−3.3	Extended	α	7.8/10	Point	165 μsec
3	^{224}Ra	α	5.8/10	Point	α	6.4/10	Point	55 sec
4	^{220}Rn	α	6.4/10	Point	α	6.9/10	Point	0.15 sec
5	^{212}Bi	$\beta^- + \gamma$	0−2.2	Extended	α	8.9/10	Point	305 nsec
6	^{212}Bi	α	6.2/10	Point	$\beta^- + \gamma$	3.2-5.0	Extended	3.1 min

2) Uniqueness of Reaction Tags and Vetoes: The signatures for ν reactions and vetoes against background are based on several properties specifying the tag. These fingerprints must be specific enough that the tags can be operated without interference from each other. Particularly, a signature tag should not be confused with a rejection tag. Tables A3 and 9 show that it this is indeed the case. In one possible case, the $(\overline{\nu}_e, p)$ tag (Table 10) may appear superficially similar to the fast (β,α) veto in the decay of ^{212}Bi (Table A3) since the visible α energy (890 keV) can, occasionally, be confused with the 480 keV γ of the former. However, any interference is avoided by additional criteria: (i) PSD can identify the α and (ii) the the initial β^+ energy of the $(\overline{\nu}_e, p)$ reaction ($E_{\beta_+} > 2.5$ MeV) excludes the ^{212}Bi events which have $E_{\beta^-} < 2.2$ MeV.

3) Alpha and Neutron-induced Reactions: The presence of α's in the B-containing FV calls for consideration of α-induced reactions since ^{10,11}B present low thresholds to these reactions (^{16}O and ^{12}C are inert to U/Th α's). The main channels are (α,n and$n\gamma$), (α,pγ) and secondary (n,n'γ). Since level energies of the product nuclei from these reactions are 3-5 MeV, these γ-rays lie close to the Nuex signal. The (n,n'γ) on ^{11}B from the secondary neutrons can, in principle, produce the very γ-rays of the Nuex signal.

The total cross-sections for α reactions on light elements and on B have been extensively studied: [(α,n),[32] B(α,n),[33] [34] [35] and B(α,pγ)[36]]. The thick-target neutron yield in a boron target by 5.3 MeV α's is [33] 19n/$10^6\alpha$'s. This applies to the uncorrelated α's (40%) in Borex, all of which have energies $<$5.5 MeV. The n yield from O and C are negligible. Thus, with 18.7% B and 1500 uncorrelated α's/day in the FV, the n-yield is $\sim 5\text{x}10^{-3}$ n/day. The only γ-ray producing reactions with thresholds open to these α energies are: ^{10}B(α,pγ)^{13}C*(3.1, 3.68 and 3.85 MeV) (Q$>$0) and ^{10}B(α,dγ)^{12}C*(4.4 MeV) ($E_{thr}=-4.26$ MeV). The latter is not important because the α energies are barely over threshold and the cross-section is low. The cross-section for the (α,pγ) reaction is, however, comparable to that of (α,n) at these energies.[34] [36] Even so, the maximum total γ-yield from (α,pγ) can be only $5\text{x}10^{-3}$ γ's/day at 3 to 4 MeV, negligible compared to the Tl remnant in Fig. 10.

The remaining 60% of the α's which occur only as correlated events (Table A3) have typically higher energies, with an average n-yield about twice that at 5.3 MeV. They thus produce $\sim$0.015n/day, still a small yield. The (α,nγ) yield is only $\sim$10% of this. Further, these α induced reactions can be tagged and vetoed efficiently by the correlated α's or $\beta+\gamma$ events appearing with short time delays (see Table A3) before or after the reaction. This is particularly true for the (n,n'γ) events which need at least 4-5 MeV neutrons that can be produced only by high energy α's from Bi decays. In addition to these correlated tags, reactions with neutron end-products can be globally tagged by the delayed coincidence signal of n-capture by B. Thus, except for the small (α,pγ) contribution, α-induced reactions produce little background, in general, in Borex.

Appendix III. Correlated Events II: Muon Induced Activity

1) Muons Underground: The intensity of muons vs. underground depth has been well studied. Experimental intensities at the three underground sites of interest to Borex are given in Table A4. Throughgoing muons (TGM) deposit some 2 GeV in the detector. Producing $\sim$300 pe/PMT, the muon track can be determined with high precision both by timing and by pin-pointing the entry and exit points which receive a marked excess of hits. The precise track resolution achievable in Borex must await simulation studies; however, a 1σ radius of 10-15 cm for the reconstructed track cylinder appears reasonable. Stopped muons (StM) can be identified immediately by the lack of an exit point. The scintillation light from a TGM should drop below threshold in $\sim$2 μsec, assuming that the slow decay component for muons is similar to that for electrons (see§5). Thus primary muons can be vetoed with negligible dead-time.

Table A4. Muon-related Rates at Underground Laboratories

Det./ Site	Obs. Rate (μ/sec)	Proj. Area (m^2)	μ Rate /m^2sec	Borex Area (m^2)	μ (Borex) /day	StM /day	μIA /day
IMB	2.8	400	$7\text{x}10^{-3}$	130	$0.8\text{x}10^5$	800	80
K-II	0.32	160	$2\text{x}10^{-3}$	65	$1.1\text{x}10^4$	113	11
GSL			10^{-4}	130	1130	11	1.1

2) Muon Induced Activity (μIA): The main interest in muons arises, however, from the *delayed* radiations induced by muon interactions in the detector. Besides that from μ-decay (2.2 μsec) (StM only), the more significant delayed radiations arise from μIA such as: i) μ^- capture with or without particle emission (StM only); ii) spallation (mainly from TGM) and iii) secondary reactions of particles emitted in i) and ii). Time-delays upto several min may be associated with these μIA species. Because of the long delays, the dead-time for vetoing delayed radiation becomes significant, ultimately deciding the underground depth necessary for Borex.

A list of *all* the possible μIA species with ^{16}O, ^{12}C and ^{10,11}B as targets, the μ interactions generating them and the resulting radiations are given in Table A5. Not all of them are important. Secondary reactions in general, contribute 2 to 3 orders of magnitude fewer μIA. This leaves μIA species of mass $\leq$16 from ^{16}O, ^{12}C, ^{11}B and ^{10}B. The dominant source of μIA is *oxygen*. The presence of C and B in addition, as in Borex, does not result in any μIA not already made from O. Those with small ($<$4 MeV) energy release, neither interfere with the ν signals nor markedly increase the low energy background in the FV.

Table A5. Muon Induced Activities on ^{10}B, ^{11}B, ^{12}C, ^{16}O.

Nucl.	$T_{½}$	Q MeV	Rad.	Spall.?	μ-Cap.?	Sec. Reactn.?
$\tau<1$ s						
^{8}Li	0.84 s	16	β^-	Yes	Yes[^{12}C(μ,α)]	Yes[^{11}B(n,α)]
^{8}B	0.77 s	15	β^+	Yes	No	No
^{9}Li	0.17 s	13.6	β^-	Yes	No	No
^{9}C	0.13 s	16	β^+	Yes	No	Yes[B (p,2n +3n)]
^{12}B	20 ms	13.4	β^-	Yes	Yes[^{16}O(μ,α),^{12}C(μ)]	Yes[^{12}C(n,p)]
^{12}N	11 ms	17.4	β^+	Yes	No	Yes[B (α ,2n +3n),^{12}C(p,n)]
^{13}B	19 ms	13.4	β^-	Yes	No	No
^{15}C	2.4 s	9.77	β^-	No	Yes[^{16}O(μ,p)]	No
^{18}Ne	1.5 s	4.5	β^+	No	No	Yes[^{16}O(α,2n)]
$\tau>>1$ s						
^{10}C	19.4 s	3.61	β^+	Yes	No	Yes[B (p,n +2n)]
^{11}Be	13.8 s	11.5	β^-	Yes	Yes[^{11}B(μ),^{12}C(μ,p)]	Yes[^{11}B(n,p)]
^{16}N	7.2 s	10.4	β^-	No	Yes[^{16}O(μ)]	Yes[^{16}O(n,p)]
^{19}Ne	17.5 s	3.24	β^+	No	No	Yes[^{16}O(α,n)]
$\tau>1$ min						
^{11}C	20.3 min	1.98	β^+	Yes	No	Yes[^{11}B(p,n),^{12}C(n,2n)]
^{13}N	10 min	2.2	β^+	Yes	No	Yes[B (α,n+2n),^{12}C(d,n)]
^{14}O	1.2 min	5.14	β^+	Yes	No	Yes[^{12}C(α,2n)]
^{15}O	2 min	2.76	β^+	Yes	No	Yes[^{16}O(n,2n),^{12}C(α,n)]
^{17}F	1.1 min	2.76	β^+	No	No	Yes[^{16}O(d,n)]

Data obtained at K-II[5] indicate that $\sim$1% of the muons stop in the FV. The StM rates, scaled for Borex, are included in Table 10. Only a few of the StM undergo capture. Since every StM can be tagged, the μIA created by capture can be completely vetoed by applying a veto around the track of every StM for a certain duration. As the StM rates are relatively small and the StM tracks localizable to a fractional volume $\Delta V/V<1\%$, a routine StM veto is inexpensive in dead-time even with long veto times.

The remaining μIA, created by *spallation* and with energy release >4 MeV, are relevant for the operation of Borex. They are listed in Table A6. Most of them have lifetimes <1 sec and some of these have been observed in K-II.[5] However, two cases, ^{11}Be (13.8 sec) and ^{14}O (71 sec) have much longer lifetimes. Their radiations are below the trigger threshold at K-II but in Borex they are fully visible.

3) Borex at GSL: Is it possible to remove the ^{14}O and all other μIA as well, by a $\sim$5 min. veto on events in the track cylinder of every muon? Consider GSL with the lowest μ rate of 1130/d. A 5 min veto within a track volume $\Delta V/V$ (3σ)$\sim$1% following every muon, implies an overall dead-time fraction of $\sim$4%. Even if the ^{14}O production rate equals the *total* rate of μIA's, 1/d (scaled from the data of K-II),[5] the surviving ^{14}O will be $<$0.02/d vs. 0.36/d for the Nuex signal. This implies vanishingly small ^{14}O events under the Nuex lines since the ^{14}O spectrum is very similar to that of ^{208}Tl (Fig. 9). Thus, operation of Borex at GSL should be safe from interference from μIA's.

Table A6. Muon Induced Spallation Activities Relevant to Borex

Species	$T_{½}$	Q (MeV)	Radiations	(Target) Spall. Products
^{8}Li	0.84 sec	16	β^-	(^{16}O)5p3n; (^{12}C)3pn; (^{11}B)2pn; (^{10}B)2p
^{8}B	0.77 sec	15	β^+	(^{16}O)3p5n; (^{12}C)p3n; (^{11}B)3n; (^{10}B)2n
^{9}Li	0.17 sec	13.6	β^-(25%); β^-+n(75%)	(^{16}O)5p2n; (^{12}C)3p; (^{11}B)2p
^{9}C	0.13 sec	16	β^++p	(^{16}O)2p5n; (^{12}C)3n
^{12}B	20 msec	13.4	β^-	(^{16}O)3pn
^{12}N	11 msec	17.4	β^+	(^{16}O)p3n
^{13}B	19 msec	13.4	β^-	(^{16}O)3p
^{11}Be	13.8 sec	11.5	$\beta^-+\gamma$	(^{16}O)4pn
^{14}O	71 sec	5.1	β^++γ	(^{16}O)2n

4) Borex at Shallower Depths--Tagging ^{11}Be and ^{14}O: At K-II and IMB, the higher μ rates imply increasingly high dead-times for a global veto on TGM's. If ^{11}Be and ^{14}O can be *tagged,* then a TGM veto of only $\sim$5 sec is needed for removing all the other μIA's, thus raising the ceiling on the μ rate. Studies at K-II[5] show that the short-lived B and Li μIA can be tagged by the event energies which are characteristically much higher than for minimum ionizing TGM's. Table 11 shows that these μIA's always involve multiparticle ^{16}O spallations, probably with pion emission. Since a 5-particle spallation is the only way to produce ^{11}Be, it could be tagged efficiently by this method. However, 2n stripping and thus ^{14}O, can result from gentler μ interactions which can escape such a tag. Instead, a new method, valid only in Borex, could utilize *neutron detection* by delayed coincidence since ^{14}O involves emission of two neutrons. The tag may be practical because, with $\sim$15 MeV/n, the n-diffusion times may be $\sim$10 μsec, longer than the $\sim$2 μsec needed to drain away the photons from the muon event. Borex at Kamioka depths may be at the threshold of feasibility. Further studies on tagging ^{14}O and especially, data on muon yields of ^{14}O are badly needed. A possible way to the latter is the study of ^{14}O yields from *GeV electrons.*

Appendix IV. Neutrino and Antineutrino Background

1) Neutrino "Background": The FV contains O and C isotopes and ^{10}B besides the solar neutrino target ^{11}B. Thus an estimate of the interfering Nuex and inverse β signals from them is necessary. The main isotopes, ^{16}O (99.76%) and ^{12}C (98.9%) are almost inert to solar signals since their inverse β thresholds are $>$13 MeV, near the end point of the solar ν spectrum. This is the case also for Nuex transitions. Thus only the rare isotopes come into this consideration.

Thresholds for ^{17}O (0.037%), ^{18}O (0.2%) and ^{13}C (1.1%) are very similar to ^{11}B and are thus in the sensitive range of solar ν's. In fact, solar neutrino detection by ^{13}C (Nuex and inverse β closely similar in properties to ^{11}B)[37] and ^{18}O (inverse β ($1^+ \rightarrow 0^+$) to the 1.04 MeV state)[38] has been previously considered because of the possibility, in principle, of obtaining large amounts of *isotopically separated* ^{13}C and ^{18}O targets. In Borex however, we estimate that these two cases can contribute at the most 1% each to the inverse β signal because of their low natural abundances.

^{10}B occurs to the extent of 20% in boron. Nuex transitions ($3^+ \rightarrow 2^+$) to the 5.16 and 7.48 MeV levels in ^{10}B and inverse β transitions to the corresponding 2^+ levels in ^{10}C are possible. However, radiative data to the 5.16 MeV level[39] show that the Nuex probability should be vanishingly small; also, the deexcitation signal will be an undetectable α particle. The Nuex strength to the 7.48 MeV level is large but the solar signal is small because of the higher energy. It also decays mainly by emission of a low energy ($<$2 MeV) α. The inverse β strengths to the mirror levels can be estimated from these radiative data as in Appendix I. The only possibility is a transition to a yet undocumented level around 7.5 MeV in ^{10}C. With an effective threshold of 11 MeV, a significant solar signal is not expected. We thus conclude that the contamination of solar signals from other material besides ^{11}B in the Borex FV can be 1 to 2% at worst, mostly in the inverse β channel.

2) Antineutrino Background:

None of the target nuclei in the FV besides free protons have cross-sections for inverse β^+ reactions induced by $\overline{\nu}_e$'s that are high enough to compete with that of protons. However, a background in this case can arise from *a non-solar* $\overline{\nu}_e$ *flux,* specifically of two types, that originate from local sources. The first is due to terrestrial radioactivity. The highest energy of the $\overline{\nu}_e$ in this case is 3.3 MeV from the β-decay of ^{214}Bi in the decay chain of natural ^{238}U. This $\overline{\nu}_e$ flux can be considerable at enegies $\sim$1 MeV.[40] [41] Above the 3.3 MeV cut-off, interference due to this background is minimal. Thus, a restriction of the kinetic energy of the β^+ from the ($\overline{\nu}_e$,p) reaction to $T^+ > 1.5$ (i.e. to $\overline{\nu}_e$ energies $E_{\overline{\nu}_e} > (1.5+1.8) = 3.3$ MeV), is necessary as used in Fig. 3.

The second local source of $\overline{\nu}_e$'s is from nuclear power reactors. The $\overline{\nu}_e$ spectrum extends well beyond 3 MeV and is represented in Fig. A2, taken from Avignone.[42] The line is an analytical parametrization of these data,[43] the area under the curve being =6, the average number of $\overline{\nu}_e$ per fission in the reactor. Thus, the $\overline{\nu}_e$ event rate in Borex can be calculated by integrating the energy dependent $(\overline{\nu}_e,p)$ cross-section with the parametrized curve of Fig. A2 (normalized by the factor 6) and multiplying by Φ the total $\overline{\nu}_e$ flux from power reactors in the neighbourhood. The value of Φ at Grans Sasso has been estimated to be $\Phi=4.5\text{x}10^5/\text{cm}^2\text{sec}$.[41] The result, using a lower limit of integration of 3.3 MeV, is indicated in Fig. 3 by the notation (Terr. $\overline{\nu}_e$). This limiting background is sufficiently low that a wide range of ν lifetimes/(ν-Majoron coupling constants) can be probed by a search for the presence of antineutrinos from the sun.

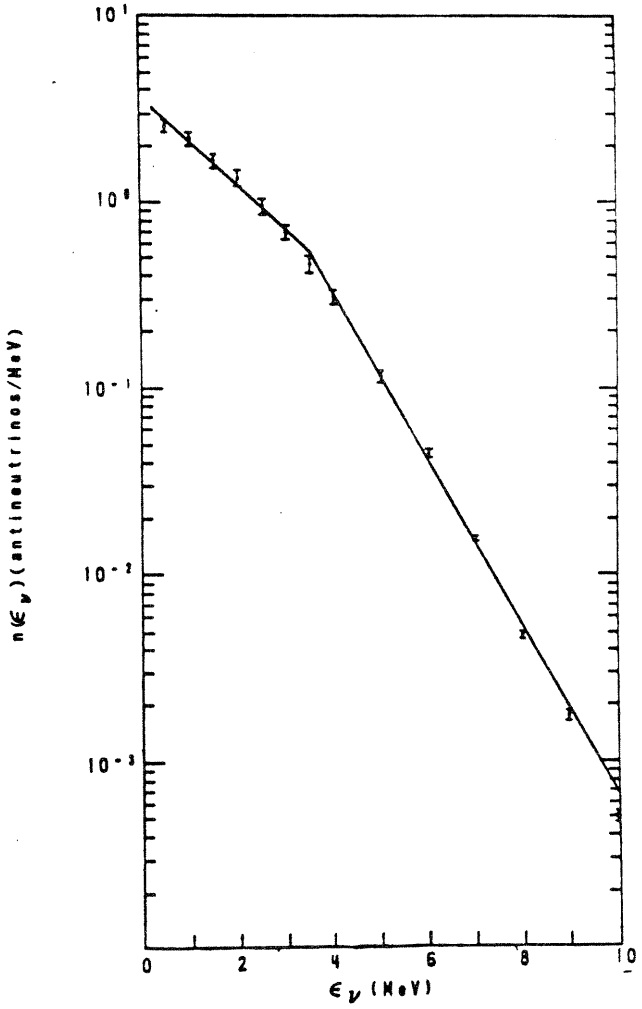

Fig. A2 Spectrum of Antineutrinos from A Nuclear Reactor (from ref. 43).

Appendix V: Light Guides for Borex

The geometrical optics of the light guides (LG) is shown in Fig. A3. The LG is a surface of revolution of a circular arc about an axis parallel to its chord. The length of the LG is L, the aperture, h, the width at its waist W and the radius of curvature of the generating arc, R. The arc subtends a half angle θ, which is the slope angle at the entrance of the LG. The LG is immersed in glycerol of refractive index n_g=1.47 and abuts the IV (n_{TPX} of the IV wall is $\approx n_g$). The TMBX scintillator has n_t=1.41.

The construction of the LG is set by the following requirements: a) The LG has a field of view of 180° into the IV and rays from the inner skin of the IV are detected with $\leq$3 reflection in the LG; b) those from the FV are detected with $\leq$2 reflections. The object is to find the angle θ such that the LG has the minimum waist width W. Referring to Fig. A3, condition b) is satisfied if the extreme ray with the double-arrow originates tangential to the FV boundary as illustrated in Fig. A4.

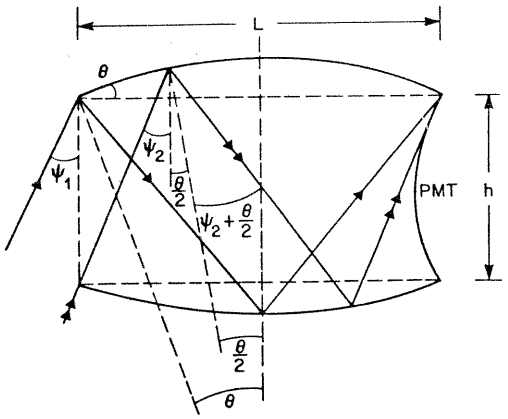

Fig. A3. Geometrical Optics of the Borex Light Guide

The angle ψ_2 in the LG for a ray that originates tangential to the FV is given by:

$$\psi_2 \;=\; \cos^{-1}(0.96\,\cos\,\psi_2{}')+\epsilon \qquad \text{(A6)}$$

where 0.96=n_t/n_g, $\psi_2{}' = \sin^{-1}(6.25/7.0) = 26.76°$ (6.25 and 7m are the radii of the FV and IV respectively), and ϵ is the tilt of the vertical at the point on the curved IV surface where the internal ray is refracted out. In the present geometry $\epsilon = 2.86°$. Thus $\psi_2 = 33.86°$. This is the minimum value of ψ_2 in the LG for a FV ray. If θ is such that this ray passes through the center of the LG after 1 bounce, then, (almost) all rays in the FV will undergo $\leq$ 2 reflections in the LG. The value of θ is set by:

$$\tan(\psi_2 + \theta) \;=\; \frac{2\mathrm{R}\sin(\theta/2)}{\mathrm{h} + 2\mathrm{R}[\cos(\theta/2) - \cos\theta]} \qquad \text{(A7)}$$

where R=L/2sinθ. With L=1.85m, h=0.46m and $\theta = 19.6^\circ$, $(\psi_2 + \theta)$=53.32° so that $\psi_2 = 33.72$. This ray will pass just outside the FV and satisfy condition b) above. Similarly, the ray with the angle ψ_1 in Fig. A3 implies ψ_1= 16.98°. An internal ray grazing the surface of the IV will be refracted into the LG with $\psi_1 = \psi'_1+\epsilon$=16.4+0.6 =17° so that it also will be transmitted with only 2 bounces. However, a grazing ray entering *the lower* edge of the LG will undergo a third bounce (see Fig. A4). Thus, rays originating between the FV and the IV wall will undergo $\leq$3 bounces, fulfilling condition a) above. In the case of large ψ, a small fraction ($\sim$1% of the total) of the rays will enter the LG grazing its curved surface and be lost as they undergo multiple large-angle bounces on the LG surface. The transmission of different rays in the LG is typified in Fig. A4. The above parameters imply a waist of W=78 cm for the LG; they can be close-packed at horizontal intervals of 5.8° and a vertical interval of 5°, so that 1450 PMT units can be used. For a nominal reflection coefficient of 0.9, an average transmission of $\sim$85% can be obtained for the FV rays (0,1 or 2 reflections) and $\sim$78% for all rays in the inner shield (0-3 reflections).

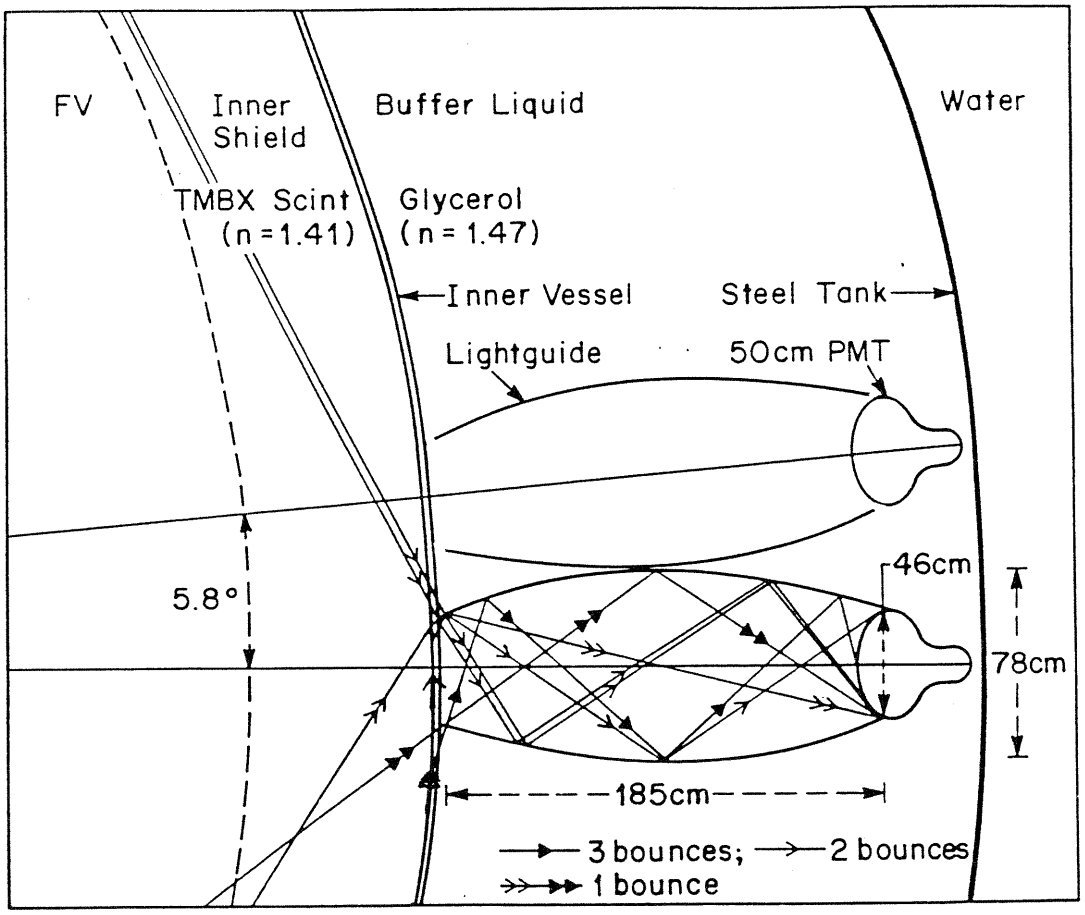

Fig. A4. Light Guide Geometry in Borex CD.

Appendix VI: New Methods for Determination of U, Th and Rn

1) Isomer Spectroscopy of Activated Nuclei (ISAN):[16] In this section, several new methods for ultrasensitive detection of U and Th *in the 100 attogram range* (1 ag = 10^{-18}g) in 1-10g samples of materials are proposed. Such sensitivities, achieved without the need of prior concentration or other processing of the sample, exceed those of current methods by several orders of magnitude. ISAN thus promises to be a major new tool for determination of U and Th in general and in boron liquid scintillators, in particular. The basic principle of ISAN is the detection of *isomeric* nuclear species (with lifetimes in the 100nsec range) by *delayed-coincidence* spectroscopy of β activities produced by slow or fast neutron activation of ^{238}U and ^{232}Th. The key to the major improvement in the sensitivity expected in ISAN is the very low background facilitated by delayed coincidence detection.

a) Determination of U by ISAN-^{239}Np*:* A standard method for the determination of ^{238}U is counting γ-rays of ^{239}Np produced by slow neutron activation of U in a reactor. With high-resolution Ge detectors, the ambient backgrounds for this method are such that $\sim 10^{-10}$g of U can be detected. The ISAN method applied to ^{239}Np can detect $<$50 ag of U in a 1g sample.

The Np is produced by the reaction:

$$^{238}\mathrm{U}\ (\mathrm{n},\gamma) \rightarrow\ ^{239}\mathrm{U}(\tau{=}2000\mathrm{sec})\beta^- \rightarrow\ ^{239}\mathrm{Np}(\tau{=}3.4\mathrm{d})\beta^- \rightarrow\ ^{239}\mathrm{Pu} \qquad \text{(A8)}$$

A 1-day irradiation of ^{238}U at a slow neutron flux of 5x10^{14}n/cm^{2}sec, produces 2.5x10^{17} Np atoms/g U (0.82x10^{12} Bq of ^{239}Np). The β^- decay of ^{239}Np populates an isomeric state at 0.3916 MeV in ^{239}Pu with a lifetime τ= 278.5 nsec which decays to the ground state involving the emission of low energy conversion electrons. The β^- branching to the isomer is 0.36 (80% $>$ 20 keV) and 75% of isomeric decays involve conversion electrons 40-100 keV in energy. Thus, $\sim$21% of the Np decays involve *delayed* ($\beta^- - \mathrm{e}^-$) coincidences.

Instead of counting the γ-rays of ^{239}Np, we propose to measure the delayed coincidences in the isomeric decay. The Np activity will be separated from irradiated samples by standard radiochemical methods. Possible traces of Zr, Hf and especially W activities will be removed by ion-exchange since ^{187}W can produce similar delayed $\beta^- - \mathrm{e}^-$ coincidences. The pure Np activity will be mixed with a small volume of liquid scintillator miscible with aqueous solutions. High ($\sim$100%) counting efficiencies for the $>$40 keV electrons in the Np coincidences can be expected. The delayed coincidences will be detected by observing the time correlated pulses in a time range of 1 μsec. In such an arrangement, the singles background is expected to be $<$1/sec which implies that in 2 meanlives of 6.8d, $<$0.6 random coincidences can occur. Detection of 2 delayed coincidences in this period can therefore be taken as a good signal for the

presence of Np. The "Np signal" implies the presence of $\sim$10 Np atoms and thus the determination of $\sim$*40 ag of U in 1g* of the original sample. Clearly, the sensitivity can be enhanced to detect even sub-attogram levels of U/g of sample by suitable prior concentration.

While this method is generally applicable, achievable sensitivities in boron liquid scintillator samples of interest to Borex will be $\sim$1000 times lower because of the depletion of the neutron flux by the high slow-neutron absorption of boron. The following method is designed to overcome this problem.

b) Determination of U by ISAN-^{237}U*:* In this approach, the relevant isomeric species is populated in the β^- decay of ^{237}U(τ=9.75d) created by *fast-neutron* activation of ^{238}U via the (n,2n) reaction. Since boron has only a small fast-neutron absorptivity, the fast-neutron flux, unlike in ISAN-Np, is not affected by the presence of boron. ISAN-U can thus be readily applied to boron liquid scintillators.

In the core position of a nuclear reactor where a total fast neutron flux of $5x10^{14}$n/cm^{2}sec can be obtained (as e.g. in HFBR, Brookhaven), the effective (n,2n) reaction cross section averaged over the fission neutron spectrum is 5 mb for ^{238}U(n,2n)^{237}U. A 1-day irradiation of ^{238}U produces $5.4x10^{14}$ ^{237}U nuclei/gU ($0.61x10^9$ Bq of ^{237}U). The β-decay of ^{237}U leads 98% to an isomeric level at 59.5 keV in ^{237}Np with a lifetime τ= 98 nsec, decaying to the ground state by γ or e^- emission. The $\beta^- - (\gamma + e^-)$ coincidences can thus be detected with $\sim$100% efficiency because of the low energy (59.5 keV) of the deexciting γ-rays. Practically every decay of ^{237}U leads to a delayed coincidence. Because of this, a "U signal" of 2 delayed coincidences in $\sim$20d (random coincidences are $\sim$0.6/20 d) indicates the presence of $\sim$2 U atoms. Thus the sensitivity for U determination using a 1-g sample is $4x10^{-15}$g U. With irradiations of 10-g samples of the boron liquid scintillators, routine detection U at the level of 400 ag U /g BLS, as desired for Borex, should be possible.

The sensitivity of U determination by ISAN-U, though not as high as ISAN-Np, is still more than two orders of magnitude higher than the best method available so far. It is in the range desirable for Borex and is applicable to boron materials. Also, since fast-n cross sections are small (values even as high as that for U above are not common) activities of irradiated samples in general and interfering activities in particular, should be much weaker and the radiochemical separation step is less critical for fast-n ISAN.

c) Determination of Th by ISAN-^{231}Th*:* Unlike the case of U, methods for specific determination of Th are fewer, although γ-ray counting of ^{233}Pa similar to Np γ-ray counting, has been used with similar sensitivities. ISAN-Th is based on ^{231}Th activity (τ=36.8h), produced by the reaction ^{232}Th(n,2n)^{231}Th with an effective (for fission n-spectrum) cross-section of 12 mb. With a fast-n flux of $5x10^{14}$ n/cm^{2}sec, a 1-day

irradiation of 1g of ^{232}Th produces 1x10^{15} ^{231}Th nuclei (0.77x10^{10} Bq of ^{231}Th activity). This activity populates an isomer at 84 keV in ^{231}Pa with a lifetime τ=63.5 nsec. The $\beta^- - (e+\gamma)$ delayed coincidences via the isomeric level occur with a branching of 0.75/decay of ^{231}Th. Thus a "Th-signal" of 2 coincidences/3d indicates the presence of $\sim$3 Th atoms, leading to the detection sensitivity of 3.3x10^{-15}g Th/g of the Boron liquid scintillator sample. A sensitivity of 330 ag Th/g of BLS, desirable for Borex, can be achieved using a 10-g sample of the BLS. In practice, both the U and Th activities will be produced in a fast-n irradiation of a sample of BLS, allowing ISAN determination of both U and Th with the same irradiation.

The ISAN approaches proposed above thus promise simple and sensitive methods for routine assay of U and Th in BLS at the level of 3x10^{-16}g of U/Th/g of BLS, the range directly relevant to Borex, using only small samples ($\sim$10 g) of scintillator liquid without concentration or other contaminating procedures.

2) On-Line Determination of Rn from BLS Liquids: In addition to the determination of long-lived ^{238}U and ^{232}Th, it is also necessary to separately determine the Ra isotopes (^{226}Ra (τ=2311 y) and ^{228}Ra (τ=10 y) which can be in disequilibrium with the U and Th decay chains. The latter is especially important since the main Nuex background in Borex due the ^{208}Tl, follows ^{228}Ra in the decay chain. Ra can be detected by separating its daughter, the noble gas radon (Rn) (denoted thoron (Tn) in the thorium chain) and counting the Rn(Tn) or its successors in the decay chain by α emissions. In the case of ^{222}Rn (τ=5d), this is relatively simple because of the long time available for removing the Rn (say by purging with He and collecting it in a trap) and counting it in a manner analagous to the Davis method for Argon in the Homestake experiment. However, a similar approach for Tn(^{220}Rn) (τ=80 sec) is more difficult.

Preliminary ideas for an *on-line counting method* for separating Tn and counting its daughter decay products have been proposed.[17] The essential elements of the method are: 1) purging Tn out of the liquid scintillator; 2) ionization by α-decay of Tn ; 3) sweeping the ionized daughter such as Po, Pb or Bi in an electrostatic drift field; and 4) counting their α and β emissions by a proportional counting wire system. Thus, Tn (or Rn) can be specifically separated continuously and counted on-line on a long term (days or weeks) basis.

A possible way to realize this method in practice, is to arrange the liquid to be forced into an sprinkler array inside a vertical cylindrical vessel as part of a closed circulating system. By this means the Tn(Rn) can rapidly escape from the liquid into vapour stream. A counter-stream of He gas flowing up the vessel is maintained, carrying the Tn(Rn) into the drift chamber via a cold-trap. Whenever Tn(Rn) decays, it creates a Po or Pb ion which is drifted to the counting wires where the (α, β) from the subsequent decay can be counted.

The sensitivity of the on-line method in determining the Rn(Tn) production rate in the boron liquid scintillator can be substantially enhanced by requiring $\beta-\alpha$ *delayed coincidence* signatures in the Bi-Po-Pb decay cascades following Rn(Tn). The "Thoron signal" is the $\beta-\alpha$(8.9 MeV) cascade with a delay time τ=440 nsec and the "Radon signal" is the $\beta-\alpha$(7.8 MeV) cascade with τ=236 μsec. In the case of Ra isotopes *in equilibrium* with U/Th present at the level of 10^{-15}g/g BLS, the rates of the above signals are: Thoron: 0.26/day/tonne BLS; and Radon: 1.27/day/tonne BLS. Comparison of the observed signal rates with the U/Th concentrations determined by ISAN can reveal whether Ra is in disequilibrium with U/Th in the liquid scintillator.

REFERENCES

1. R. S. Raghavan, S. Pakvasa and B. A. Brown, Phys. Rev. Lett. *58,* 1801 (1986).
2. R. S. Raghavan and S. Pakvasa, Phys. Rev. *D37,* 849 (1988).
3. J. W. Mitchell, R. S. Raghavan, J. Barnes and J. McLaren, AT&T Bell Labs Report (November 1987) and to be published.
4. R. S. Raghavan, X.G. He and S. Pakvasa, Phys. Rev.D (to be published).
5. A. Suzuki, in *Neutrino Physics and Astrophysics (Neutrino '86),* Ed. T. Kitagaki and H. Yuta (World Scientific) (1987) p. 306
6. T. Taddeucci, priv. comm. to R.S.R.
7. J. N. Bahcall, Rev. Mod. Phys. *59,* 505 (1987).
8. F. Reines and C. Cowan, Phys. Rev. *113,* 273 (1953).
9. For a recent review of such processes see, J. E. Kim, Phys. Rep. *150,* 126 (1987).
10. R. S. Raghavan, (unpublished) Priv. Comm. (1988).
11. J. B. Birks, *Theory and Practice of Scintillation Counting* (Pergamon) 1964.
12. R. S. Raghavan, (unpublished results) 1981.
13. R. Steinberg et al, Drexel Univ. Preprint, (1987).
14. W. H. Schechter, U. S. Patent #2891086 (1960).
15. W. R. Kelly and J. D. Fasset, Anal. Chem. *55,* 1040 (1983).
16. R. S. Raghavan, (unpublished), Priv. Comm. (1988).
17. R. S. Raghavan, J. G. Kay, R. Steinberg and C. E. Lane, (unpublished), Priv. Comm. (1988).
18. E. Beiere, priv. comm.
19. R. C. Allen et al, SNO Proposal Annex-6 (1987).
20. R. C. Svoboda, Thesis, Univ. Hawaii (1985).
21. Sudbury Neutrino Observatory Proposal (1987).

22. R. Steinberg and C. Lane (Priv. Comm.) (1988).

23. The transit time spread (FWHM) of the Hamamatsu 50 cm dia. PMT R1449 used in K-II is $\sim$9 nsec, corresponding to τ_j=3.8 nsec A value of 6.5 nsec, (τ_j=2.75 nsec) has been measured for the newer PMT R1449Z (SNO Proposal, 1987).

24. E. Bellotti, M. Buraschi, E. Fiorini and C. Liquori, INFN preprint INFN/TC-85/19 (1985).

25. L. V. Spencer and U. Fano, Phys. Rev. *81,* 464 (1951).

26. See e.g., E. Segre, *Nuclei and Particles,* (Benjamin), p. 590.

27. Sudbury Neutrino Observatory Report, (1985).

28. S. Raman et al, Nuc. Data Table, *21,* 567 (1978).

29. Fay Selove, Nucl. Phys. *A336,* 1 (1980).

30. Brown and Wildenthal, Phys. Rev. *C28,* 2397 (1986).

31. D. H. Wilkinson, Priv. Comm. to R.S.R. (1987).

32. Y. Feige, B. G. Oltman and J. Kastner, J. Geo. Res. *73,* 3135 (1968).

33. R. L. Walker, Phys. Rev. *76,* 244 (1949).

34. T. W. Bonner, A. A. Kraus, J. B. Marion and J. P. Schiffer, Phys. Rev. *102,* 1348 (1956).

35. L. van der Zwan and K. W. Geiger, Nucl. Phys. *A246,* 93 (1975).

36. S. J. Wilson, Phys. Rev. *C11,* 1071 (1975).

37. R. S. Raghavan, *Proc. PANIC, (Kyoto, 1986),* Nucl. Phys. B (in Press).

38. W. C. Haxton, Nucl. Inst. Meth. *A264,* 37 (1988).

39. F. Selove, Nucl. Phys. *413,* 134 (1984).

40. L. M. Krauss, S. Glashow and D. N. Schramm, Nature *310,* 191 (1984).

41. P. O. Lagage, Nature *316,* 420 (1985).

42. F. T. Avignone, Phys. Rev. *D2,* 2609 (1970).

43. H. C. Lee, Nucl. Phys. *A294,* 473 (1978).